Shannon Entropy of Transport Self-Organization Due to Dissolution/Precipitation Reaction at Varying Peclet Number in an Initially Homogeneous Porous Media

Evgeny Shavelzon[1] and Yaniv Edery[2]

[1,2]Technion – Israel Institute of Technology, Haifa, Israel

Correspondence: Evgeny Shavelzon (eshavelzon@campus.technion.ac.il)

Abstract. Dissolution and precipitation processes in reactive transport in porous media are ubiquitous in a multitude of contexts within the field of Earth sciences. In particular, the dynamic interaction between the reactive dissolution / precipitation processes and the solute transport is of interest, as it is capable of giving rise to the emergence of preferential flow paths in the porous host matrix. It has been shown that the emergence of preferential flow paths can be considered a manifestation of transport self-organization in porous media, as they create spatial gradients that distance the system from the state of perfect mixing and allow for a faster and more efficient fluid transport through the host matrix. To investigate the dynamic feedback between the transport and the reactive processes in the field and its influence on the emergence of transport self-organization, we consider a two-dimensional Darcy-scale formulation of a reactive transport setup, where the precipitation and dissolution of the host matrix are driven by the injection of an acid compound, establishing local equilibrium with the resident fluid and an initially homogeneous porous matrix, composed of a calcite mineral. The coupled reactive process is simulated in a series of computational analyses employing the Lagrangian particle tracking (LPT) approach, capable of capturing the subtleties of the multiple scale heterogeneity phenomena. We employ the Shannon entropy to quantify the emergence of self-organization in the field, which we define as a relative reduction in entropy, compared to its maximum value. Scalability of the parameters that characterize the evolution of the reactive process in an initially homogeneous field with the Peclet number is derived using a simple one-dimensional ADRE model with a linear adsorption reaction term, and then confirmed through numerical simulations, with the global reaction rate, the mean value and the variance of the hydraulic conductivity distribution in the field all exhibiting dependency on the reciprocal of the Peclet number. Our findings show that transport self-organization in an initially homogeneous field increases with time, along with the emergence of the field heterogeneity due to interaction between the transport and reactive processes. By studying the influence of the Peclet number on the reactive process, we arrive at a conclusion that self-organization is more pronounced in diffusion-dominated flows, characterized by small Peclet values. The self-organization of the breakthrough curve exhibits the opposite tendencies, that are ~~explained from the thermodynamic perspective~~ observed from the perspective of a thermodynamic analogy. The hydraulic power, required to maintain the driving head pressure difference between the inlet and outlet of the field, was shown to increase with the increasing variance, as well as the mean value of the hydraulic conductivity distribution in the field, using a simple analytic model. This was confirmed by numerical experiments. This increase in power, supplied to the flow in the field, results in an increase in the level of transport

self-organization. Employing thermodynamic framework to investigate the dynamic reaction-transport interaction in porous media may prove beneficial whenever the need exists to establish relations between the intensification of the preferential flow path phenomenon, represented by a decline in the Shannon entropy of the transport, to the amount of reaction that occurred in the porous medium and the change in its heterogeneity.

1 Introduction

1.1 Dissolution/precipitation reaction and preferential flow paths in porous media

Dissolution and precipitation processes in reactive transport in porous media play an important role in multiple contexts in the field of Earth sciences, such as geological CO_2 storage [Ajayi et al. (2014)], reactive contaminant transport [Brusseau (1994)], and acid injection in petroleum reservoirs [Shazly (2021)]. They are responsible for alteration of the transport characteristics of the porous media and emergence of preferential flow paths [Singurindy and Berkowitz (2003), Al-Khulaifi et al. (2017)], as dissolution / precipitation reactive processes lead to changes in the dimensions of the pores and their connectivity, thus introducing coupling between the chemical reaction and the transport in the media. This is observed, for example, in reactive infiltration in a porous medium, where chemical reaction at the solid-fluid interface causes dissolution of the surrounding porous matrix, creating nonlinear feedback mechanisms that often lead to greatly enhanced permeability [Ladd and Szymczak (2021), Szymczak and Ladd (2006)]. The solid-fluid interface instability, observed in this case, is similar to the viscous fingering phenomenon in the field of multi-phase flow, with undulation areas formed first at the solid-fluid interface of the porous media due to dissolution, which are later transformed into well-defined finger-like channels or wormholes, that rapidly advance into the medium. As dissolution proceeds, these fingers interact, competing for the available flow.

These wormholes that funnel the flow can be regarded as preferential flow paths, ubiquitous in heterogeneous porous media, where most of the transport is concentrated. The importance of preferential flow paths in determining the transport properties of the porous media is widely recognized, as they allow rapid solute transport and alter residence times [Beven and Germann (1982), Stamm et al. (1998), Radolinski et al. (2022), Edery et al. (2014), Edery et al. (2016a)]. As these preferential flow paths align with the average flow direction, they introduce solute concentration gradients in the direction transverse to flow [Zehe et al. (2021)] and an increasingly non-Fickian transport behavior, thus requiring a global homogenization approach for transport characterization that considers these subtleties in the upscaling / volume averaging methods. The formation of preferential flow paths in the porous matrix due to interaction between dissolution reaction and transport processes has been reported in a multitude of experimental studies [Kamolpornwijita et al. (2003), Zhang et al. (2021), Snippe et al. (2020), Li et al. (2019)], while the opposite scenario of a precipitation reaction, such as in the formation of carbonate deposits during CO_2 sequestration, was investigated by Yan et al. (2020); they reported clogging of pores, leading to alteration or complete blockade of the preferential flow paths. As opposed to the case of highly conductive networks, such as fractured rock formations, the preferential flow paths in the saturated heterogeneous porous media are not always well defined. For this case, Zehe et al. (2021) have reported that a higher variance in the hydraulic conductivity field leads to the intensification of the preferential flow path phenomenon via a

stronger concentration of solute within a smaller number of paths. Changing the observing perspective, [Berkowitz and Zehe (2020)] have argued that the emergence of preferential flow paths can be viewed as a manifestation of self-organization, as the spatial concentration gradients, created within the system, distance the system from the state of perfect mixing, thus allowing for a faster and more efficient fluid transport.

1.2   Self-organization in physical systems and thermodynamic framework

The findings discussed above have brought us closer to classification of the emerging preferential flow paths in reactive transport in porous media as an embodiment of self-organization. Before addressing the specific problem of the emergence of preferential flow paths, it is in order to first discuss some basic concepts related to the phenomenon of self-organization in physical systems. Self-organization refers to a broad range of pattern-formation processes, occurring through interactions internal to the system, without intervention by external directing influences [Camazine et al. (2001)]. Examples of self-organization in physical systems include formation of patterns in chemical reactions [Turing (1952)], animal behavior, such as bird flocking [Hemelrijk and Hildenbrandt (2012)] and river network formation [Stolum (1996)]. In this context, it is interesting to consider reaction-diffusion systems, that have attracted much interest as a prototype model for pattern formation in nature. An attempt to provide an explanation of morphogenesis in the field of mathematical biology was first made by Alan Turing [Turing (1952)], that proposed a model based on chemical reaction-diffusion interaction, where two homogeneously distributed substances interact to produce stable stationary patterns, represented by concentration deviations of the two substances inside the domain of the reaction. The reaction is autocatalytic and is represented by a system of nonlinear differential equations, thus possessing the capability for exhibiting self-organizing modes. The necessary condition for pattern emergence requires that diffusion coefficients of both substances differ, otherwise no self-organization will take place. This feature counteracts the homogenizing action of diffusion. Turning to the field of hydrology, Berkowitz and Zehe (2020) have stated that, while self-organization in well-defined networks, such as rivers, is clearly distinguishable, nevertheless also the cases that lack well-defined network, such as transport in heterogeneous groundwater systems in the absence of fractures, are capable of displaying some characteristics of self-organization, that is manifested through spatially correlated, anisotropic patterns of structural and hydraulic properties.

Within the thermodynamic framework, Haken (1983) has defined self-organization as an emergence of ordered macroscale states in an open, complex system, far from thermodynamic equilibrium due to exchange of energy and matter with surroundings, as a result of a synergetic interplay of microscale, irreversible processes. Recall the definition of entropy by Boltzmann, that is directly related to the number of possible microstates of a system that are consistent with a given macrostate, characterized by the macroscopic thermodynamic properties of the system [Haken (1983)]. An ordered state is characterized by a reduction in entropy of the system, compared to its maximum value at equilibrium, thus, a macrostate with a lesser amount of corresponding possible microstates is considered more ordered [Kondepudi and Prigogine (1998)]. Since, according to the 2nd law of Thermodynamics, the overall entropy of the system and its surroundings cannot decrease, this reduction in entropy has to be exported from the system outside, leading to an increase in the entropy of its surroundings. The export of entropy from the system requires that physical work is performed on the system in order to maintain the current level of self-organization. One

of the most exciting examples that come to mind to illustrate this concept is biological life. Erwin Schrodinger in his highly influential book *What is Life?* [Schrodinger (1944)] describes a living organism as a non-equilibrium thermodynamic system in interaction with its surroundings, that maintains a level of inner self-organization. How does a living organism manage to avoid decay into the inert state of equilibrium? The answer is simple: by consuming food and transforming it into energy through metabolic processes. This energy allows the organism to maintain its level of self-organization by exporting the entropy, produced by irreversible physiological processes, to the surroundings. In other words, in order to maintain self-organization within a living organism, it works to decrease the level of self-organization of its surroundings by exporting entropy outside.

While the thermodynamic framework refers to physical entropy, introduced by Clausius (1857), the information entropy, first defined by [Shannon (1948)], has proven to be extremely useful in quantifying self-organization in various fields of physical science. This parameter, also referred to as the Shannon entropy, was introduced originally in the framework of communication. Viewing communication as a statistical process, Shannon employed an entropy-like parameter, defined similarly to Boltzmann's definition of entropy, to provide a measure for the amount of transmitted information, carried by a certain sequence of symbols. The applications of Shannon entropy in the field of geophysical science are plenty; Chiogna and Rolle (2017) have employed Shannon entropy to quantify dilution and reactive mixing in solute transport problems; Schweizer et al. (2017) used it for uncertainty assessment in complex geological models; Mays et al. (2002) have measured temporal and spatial complexity of unsaturated flow in heterogeneous media; Woodbury and Ulrych (1996) have applied the minimum relative entropy principle (MRE) from the field of information theory to the problem of recovering the release history of a groundwater contaminant; Hansen et al. (2018), Hansen et al. (2023) have employed the Jaynes maximum entropy principle to determine the flow configuration for the case of immiscible and incompressible two-phase flow in porous medium. Zehe et al. (2021) has studied self-organization in preferential flow paths in porous media of various degrees of spatial heterogeneity and quantified it in terms of Shannon entropy. They found that stronger transversal concentration gradients emerge with an increasing variance of the hydraulic conductivity field, which is reflected in a smaller entropy of the transversal distribution of transport pathways. Their findings suggest that a higher variance of the hydraulic conductivity field coincides with stronger self-organization of transport pathways (represented by steepening of the concentration gradient in the direction transverse to flow). The explanation to this non-intuitive finding is given in terms of energy: in the thermodynamic framework, the emergence of spatial self-organization requires energy input into the system, which grows along with the increase in the level of self-organization. Since the energy input in the form of hydraulic power, necessary to sustain steady-state fluid flow and tracer transport, grows with the variance of the hydraulic conductivity field, this enables an increase in self-organization of the transport in the field.

1.3   Lagrangian particle approach in transport in porous media

Among the family of numerical methods employed to simulate transport and reaction problems in porous media, the Lagrangian particle approach continues to gain more prominence in the recent decades, along with the continuing development of powerful computers [Jiao et al. (2021), Sole-Mari and Fernandez-Garcia (2018), Sole-Mari et al. (2020)]. The Lagrangian family of computational methods considers the fluid phase as consisting of discrete particles and tracks the path of each par-

ticle, as opposed to the more conventional Eulerian family of methods, where the fluid phase is treated as a continuum and its governing equations are developed based on conservation principles [Zhang and Chen (2007), Meakin and Tartakovsky (2009)]. In the Lagrangian approach, motion and interaction of particles are defined by a specific set of laws that correspond to the physical situation of interest. Statistical analysis is then applied to the particle trajectories and interactions. The Lagrangian particle methods are not susceptible to numerical instabilities that are often present in the numerical simulations where an Eulerian approach is employed [Meakin and Tartakovsky (2009)]. Perez et al. (2019) employed random walk particle tracking to simulate bimolecular irreversible chemical reaction in porous media and have shown the equivalence of their formulation to the well-known advection-diffusion-reaction equation (ADRE), while others used it to simulate reactive transport in heterogeneous fields that displays non-Fickian behavior [Berkowitz et al. (2013), Edery et al. (2013), Edery et al. (2010), Edery et al. (2009), Edery et al. (2016b)]. Other applications of Lagrangian methods include particle dispersion in fluid [Shirolkar et al. (1996)], multiphase flows [Meakin and Tartakovsky (2009)], reactive transport [Schmidt et al. (2019)] and impact problems, such as water impingement on a surface [Petrosino et al. (2021)].

1.4 Objectives

To investigate the dynamic interaction between the transport and the reactive process in an initially homogeneous porous medium and its influence on the emergence of transport self-organization in the medium, we consider a two-dimensional Darcy-scale formulation of a reactive transport setup, where precipitation and dissolution in the medium are driven by the injection of an acid compound, establishing local equilibrium with the resident fluid and an initially homogeneous porous medium, composed of calcite mineral. The coupled reactive process is simulated in a series of computational analyses where the low pH water is injected into an initially homogeneous domain, at first in equilibrium with the resident fluid (high pH water). We employ a Lagrangian particle tracking (LPT) approach, capable of capturing the subtleties of the multiple scale heterogeneity phenomena, along the lines of Edery et al. (2021).

In particular, we are interested in the influence of the transport Peclet number on the reactive process and the emergence of self-organization of the transport in the porous medium. To investigate this relation, we simulate a number of reactive transport scenarios for different values of advective to diffusive transport rates, characterized by the Peclet number. This is achieved by applying different values of the inlet-outlet hydraulic pressure head drop boundary condition to the field. We employ Shannon entropy along the lines of Zehe et al. (2021) to quantify the emergence of transport self-organization in the medium. In Section 2 we review the basic methodology of our reactive setup approach, followed by the discussion of the concept of self-organization in the context of transport in porous medium, its quantification and relation to hydraulic power in Section 3. We present and discuss the obtained results in section 4.

2 Reaction, flow and transport modelling

2.1 Chemical reaction model

The key component in dissolution-precipitation reactions is the stoichiometric equilibrium between the reactants and the products. In the system under investigation, the simulated reactive transport scenario is that of an injected acid compound (low pH water), establishing local equilibrium with the resident fluid (high pH water) and the porous medium, composed of calcite mineral. This fairly common setting in the field of geosciences constitutes a specific case of Edery et al. (2011), where dedolomitization is also included in the chemical model (see also Singurindy and Berkowitz (2003), Al-Khulaifi et al. (2017)). When the low pH water (pH level of 3.5) enters the calcite porous medium, initially saturated and in chemical equilibrium with the resident fluid (pH level of 8), dissolution of calcite occurs, accompanied by the production of calcium and carbonic acid, as represented by the following equations

$$CaCO_{3(s)} \leftrightarrow Ca^{2+} + CO_3^{2-} \tag{1}$$
$$CO_3^{2-} + 2H^+ \leftrightarrow H_2CO_3 \tag{2}$$

Here, the carbonate ion CO_3^{2-}, that appears due to dissolution of $CaCO_3$ in water, recombines with two hydrogen ions H^+ to produce carbonic acid. The deprotonation reaction (2) represents the sum of the two acid equilibria of the carbonic acid [Manahan (2000)]. The fluid pH level is assumed to be bounded by that of the resident fluid. The reaction is assumed to be fully reversible, therefore the opposite precipitation reaction is also possible, given that the pH conditions are favorable. The injected fluid is a source of both Ca^{2+} and H^+. We assume an abundance of Ca^{2+} in the fluid, thus making the reaction (1) non rate-limiting; therefore, the rate-limiting reaction is (2), that is controlled by the available hydrogen ions H^+. This is consistent with experimental observations [Singurindy and Berkowitz (2003)]. Combining both equations along the lines of Edery et al. (2021), we obtain the following simplified equation

$$A \leftrightarrow B \tag{3}$$

where A and B represent $2H^+$ and H_2CO_3, respectively. The direction of reaction is governed by the deviation from the chemical equilibrium, as defined by the current concentrations of H^+ and H_2CO_3 in the localized area of reaction. In the presence of H^+ concentration above the equilibrium value, dissolution will occur and vice versa. While pH levels control the dissolution-precipitation reaction, the hydrogen ion concentration, that establishes the pH, is controlled by the transport processes of the invading fluid.

2.2 Flow and transport simulation

To investigate the dynamic coupling between the transport and reactive processes in the porous medium, we consider a two-dimensional field of dimensions $L_x \times L_y = 12 \times 30$ cm^2, made of calcite mineral. Here, L_x and L_y are the domain dimensions in the direction parallel and transverse to the flow, respectively. The field is assumed to be fully saturated with a resident high pH water and initially in chemical equilibrium. Low pH water is being injected at the inlet boundary, causing reaction

inside the porous medium as it advances. The field is discretized into $N_x \times N_y$ computational cells, where $N_x = 150$ and $N_y = 60$ are the number of cells in the direction parallel and transverse to the flow, respectively, each cell having dimensions of $\Delta x, \Delta y = 0.2$ cm. The field is initially homogeneous in terms of hydraulic conductivity K and porosity θ that have initial values of $K_0 = 10.9869$ cm/min and $\theta_0 = 0.4$, respectively. A hydraulic head drop boundary condition Δh_{BC} is applied between the field's inlet and outlet boundaries, while the upper and lower field boundaries are ideal (reflective) walls. The flow within the field, subject to the boundary conditions as described above, is governed by the continuity and the Darcy equations (4-5) and solved in terms of the hydraulic pressure head with the help of a Finite element method computer code (Guadagnini and Neuman (1999)). The obtained hydraulic head distribution is then converted into flow velocity at each computational cell.

$$\nabla \cdot \mathbf{q}(\mathbf{x}) = 0 \tag{4}$$

$$\mathbf{q}(\mathbf{x}) = -K\nabla h(\mathbf{x}) \tag{5}$$

Here $\mathbf{q}$ and h are the Darcy flux and the hydraulic head distributions over the field and K is the hydraulic conductivity, all functions of the field spatial coordinate $\mathbf{x}$. Here and throughout the paper bold font is used to specify vector fields, as opposed to scalar fields written in the regular font.

The solute transport across the field is simulated using a Lagrangian particle tracking approach (Le Borgne et al. (2008)). The invading fluid is represented by the reactive A particles injected into the porous medium. A total number of $N_{tot} = 5e5$ A particles, representing the available pore volume in the field at pH 3.5, is injected per pore volume time at the inlet boundary at a constant rate proportional to the mean flow velocity in the initial homogeneous field, so that in every computational time step Δt the amount of injected particles is $v_0 \cdot (\Delta t/L_x) \cdot N_{tot}$, where v_0 is the mean flow velocity magnitude within the initial homogeneous field (assuming that the change in the mean conductivity value is minor over the simulation time). The mean velocity v_0 is calculated from the applied pressure head drop over the field Δh_{BC} using Darcy's law: $v_0 = K_0/\theta_0 \cdot \Delta h_{BC}/L_x$. The particles injected at each time step are flux-weighted according to the conductivity distribution of the inlet cells. The particle injection rate is such that all of the available pore volume in the field is sampled by the particles by the time all N_{tot} of them have been injected. The time of this occurrence will be referred to as pore volume time $T_{pv} = L_x/v_0$ throughout the paper.

The injected A particles are being advanced in the field using the Langevin equation, that combines deterministic (advective) and stochastic (diffusive) contributions [Risken (1996)]. The position $\mathbf{d}(t)$ of a particle due to the combined effect of advective and diffusive transport mechanisms is described by (6), where $\mathbf{v}$ is the flow velocity field, t is the computational time, D is the diffusion coefficient of the invading fluid in the porous medium and $\boldsymbol{\xi}(t)$ is a vectorial Gaussian random variable characterized by $\langle \boldsymbol{\xi}(t) \rangle = \mathbf{0}$ and $\langle \xi_i(t)\xi_j(t') \rangle = \delta_{ij}\delta(t - t')$.

$$\frac{d\mathbf{d}(t)}{dt} = \mathbf{v}[\mathbf{d}(t)] + \sqrt{2D}\boldsymbol{\xi}(t) \tag{6}$$

An important property of Langevin equation (6) is its equivalence to the well-known advection-diffusion equation (ADE) [Risken (1996), Perez et al. (2019)]. To be used in the context of a numerical simulation, the equation is discretized using the

simple Euler-Maruyama method [Kloeden (1992)] as follows

$$\mathbf{d}_{k+1} = \mathbf{v}_k \cdot \Delta t + \mathbf{d}_D \tag{7}$$

where $\mathbf{d}_{k+1} = \mathbf{d}(t_{k+1})$ is the particle location at the current computational time step $t_{k+1} = \Delta t \cdot (k+1)$ and $\mathbf{v}_k = \mathbf{v}[\mathbf{d}(t_k)]$ is the flow velocity at the particle location at the previous computational time step $t_k = \Delta t \cdot k$ (here the index k is not to be confused with the hydraulic conductivity K). The diffusive contribution is given by $\mathbf{d}_D = \sqrt{2D\delta t} \cdot N(0,1)$, where D=1e-5 cm^2/min is the representative value of the diffusion coefficient [Domenico and Schwartz (1997)], $N(0,1)$ is a standard normally distributed random variable and $\delta t = \delta s/v$ is the time it takes a particle to move the fixed distance $\delta s = \Delta x/10$ while traveling with the flow at a speed of magnitude $v = |\mathbf{v}|$. The obtained diffusive contribution has no spatial preference, since its spatial direction is represented by a uniformly distributed random variable between $[0, 2\pi]$. The particle movement in the duration of the computational time step Δt consists of a series of jumps of a constant magnitude δs, to which the diffusive contribution is added. This series of jumps continues until their cumulative time $\sum_i \delta t_i$, where i is the jump index in the series, reaches Δt.

At first, no B particles exist in the field. After all newly injected A particles have been advanced to their current locations, they are allowed to react according to an algorithm described in Section 2.3. Following reaction, as described by (3), B particles appear in the field and the computational cell values of porosity and hydraulic conductivity in the area of reaction are being updated correspondingly, thus creating an interaction between the reactive and the transport processes. Beginning the next computational step Δt, another set of A particles is being injected into the field employing flux-weighting in accordance to the reaction-modified conductivity distribution of the inlet cells. Then, all available particles in the field (both A and B) are being advanced again and reaction occurs. Note that the diffusive contribution to particle displacement $\mathbf{d}_D$ allows for the mixing effect in the field due to its stochastic nature. Following the changes in the hydraulic conductivity field due to the reactive process, the hydraulic pressure head field and the corresponding flow velocity field are being updated at constant time intervals of $10\Delta t$ (in order to reduce constraints associated with computational costs), while the reaction is allowed to occur every Δt. The simulation continues until the pore volume time T_{pv} is reached, while the A particles injection rate remains constant throughout the simulation. Hydraulic conductivity, pressure head, porosity and velocity fields, as well as the amount of dissolution-precipitation reactions that took place in each computational cell, are recorded at constant time intervals of $10\Delta t$ as well, to be analyzed in the post-processing stage. The particle transport algorithm, along with the chemical reaction model described above, constitute two important aspects of the kinetic reaction mechanism, as implemented in the current study.

The transport part of the model has been validated against the well-known case of one-dimensional instantaneous injection in homogeneous medium, for which analytical solution exists [Kreft and Zuber (1978)]. See Appendix C in the Supplementary data for details.

2.3   Kinetic reaction mechanism

In the system under investigation, the kinetic reactive process operates accordingly to an algorithm, developed to mimic the actual chemical dissolution/precipitation reactions that take place in practice. After all existing A and B particles in the field have been advanced in the current time step, reaction is allowed to occur. Since the reaction is assumed to be locally instantaneous, at each instant of computational time Δt the reaction is allowed to proceed until local equilibrium is reached in each field cell. For that purpose, the number of currently residing particles of both kinds is assessed in each cell. Each A particle is assigned a molar amount based on the assumption that the total number of A particles injected per pore volume time N_{tot}, distributed evenly across the field, result in the pH level of 3.5 throughout the field, which corresponds to the pH level of the invading fluid. The following calculation is performed: a total available pore volume in the computational field $\theta_0 L_x L_y$ is multiplied by the molar density of the hydrogen ions that are being injected into the field, corresponding to a pH level of 3.5. This gives 4.55e-5 mol of hydrogen ions that are required to fill the initially available pore volume to obtain a pH level of 3.5 throughout the field. To obtain the molar amount assigned to a single A particle, this value is divided by N_{tot}. For $N_{tot} = 5e5$ A particles as defined in the current simulation, each one obtains a parcel of 9.1e-11 mol of H^+ (recall that $A = 2H^+$). Based on (3), each B particle obtains half of this molar amount of carbonic acid. The number of A particles in a particular cell to obtain pH 3.5 there is calculated by dividing N_{tot} particles by the number of computational cells in the field $N_x \cdot N_y$ to obtain approximately 56 (while zero A particles in a cell represents pH level of 8 there, which corresponds to the pH of the resident fluid). Based on the actual number of A particles in the cell, the current pH level there is estimated using a linear proportion from these limiting values. Since Ca^{2+} is not the rate-limiting factor, reaching local equilibrium in the cell amounts to equilibrating the carbonates there. The equilibrium value of the fractional amount of H_2CO_3 in relation to the total amount of carbonates in a cell, denoted by $\alpha_1(pH)$, is calculated based on the current pH value in the cell as

$$\alpha_1(pH) = \frac{10^{-2pH}}{10^{-2pH} + 10^{-pk_{a1}} + 10^{-pk_{a2}} + 10^{-pH - pk_{a1}}} \tag{8}$$

with the standard values $pk_{a1} = 6.35, pk_{a2} = 10.33$ [Manahan (2000)] (see Appendix A in Edery et al. (2011) for details). The value of $\alpha_1(pH)$ is then compared to the current fractional amount of H_2CO_3 in a cell, calculated based on an assumption that the total amount of carbonates in a cell at any time corresponds to the amount of H^+ that results in a pH level of 3.5 there. The direction of the reaction may now be determined in accordance with (3): dissolution will occur if the fractional amount of H_2CO_3 is smaller than the equilibrium value, and vice versa. A single reaction is allowed to occur, during which a single A particle in a cell transforms into a B particle or vice versa. After each reaction turn, the local pH level in a cell and the fractional amount of H_2CO_3 there in equilibrium $\alpha_1(pH)$ and in practice are recalculated and the reaction process is repeated until equilibrium is reached.

After that, the cell porosity θ is updated in accordance with (9), where the subscripts $k + 1$ and k denote values at the current and previous computational steps, respectively (before and after the reaction has taken place). Here, the porosity increment is actually the volume of calcite, dissolved or precipitated due to reaction, divided by the volume of the cell $\Delta x \Delta y$ (assuming unit cell depth). According to (1)-(2), the change in cell volume is equal to the change in molar amount of H_2CO_3 due to reaction

in the cell $d[H_2CO_3]$ (can be positive or negative, depending on the direction of reaction) times the molar volume of calcite, taken to be $M_{CaCO_3} = 36.93$ cm^3/mol [Morse and Mackenzie (1990)]. The porosity is not allowed to exceed limiting values of 0.01 and 0.99, set to avoid occurrence of non-physical scenarios. The hydraulic conductivity K is then updated employing the Kozeny-Carman relation (10).

$$\theta_{k+1} = \theta_k + \frac{d[H_2CO_3]M_{CaCO_3}}{\Delta x \, \Delta y} \tag{9}$$

$$K_{k+1} = K_k \cdot \frac{\theta_{k+1}^3}{(1-\theta_{k+1})^2} \cdot \frac{(1-\theta_k)^2}{\theta_k^3} \tag{10}$$

This process is repeated for each of the cells in the field before the particles are allowed to advance again in the next computational time step. In order to overcome constraints, associated with computational costs, reaction enhancement has also been considered. For this purpose, the change in the cell volume (9) due to a certain amount of reaction that took place there is increased by several orders of magnitude. This is equivalent to accelerating the reactive process in the field, while the overall dynamics, associated with the reactive process, remains the same.

2.4 Definition of the Peclet number

The Peclet number plays an important role in our reactive system. As a usual practice, Peclet number is calculated based on an Eulerian length scale, such as the mean grain or pore diameter in the pore scale simulation or the characteristic correlation length of the heterogeneous porous media for the case of the Darcy scale simulation [Nguyen and Papavassiliou (2020)]. The Eulerian definition of the Peclet number as the ratio of advective to diffusive transport rates gives the following well-known relation $Pe = \tilde{v}L/D$, where $\tilde{v}$ is the mean velocity and L is the characteristic length. This definition often yields estimates that allow little physical insight on the subject of the relative contributions of the advective and diffusive processes in the transport in porous media under investigation. Moreover, in the case of reactive transport in an initially homogeneous porous medium on the Darcy scale, such as in the current study, where heterogeneity is gradually introduced in the field, correlation length can be time-dependent; this calls for alternative approaches in defining the Peclet number, capable of giving a deeper insight into the transport characteristics. In order to find a meaningful estimate for this parameter, we attempt at formulating the expression for the Peclet number based on Lagrangian length scale quantities, noting, after Nguyen and Papavassiliou (2020), that the nature of hydrodynamic dispersion is Lagrangian. For this purpose we turn to the Langevin equation (6), which governs the particle advancement in the simulation. Each jump made by a particle during the time period δt consists of a constant value advective contribution $\delta s = \Delta x/10$ and a diffusive contribution $\sqrt{2\,D\,\delta t} \cdot N(0,1)$ (see Section 2.2). Only the magnitude of the diffusive contribution is of importance, therefore we will consider its absolute value $\sqrt{2\,D\,\delta t} \cdot |N(0,1)|$. The random variable $|N(0,1)|$ is half-normally distributed with expectation value of $\sqrt{(\frac{2}{\pi})}$ [Leone et al. (1961)]. Therefore, we are able to formulate the expression for the Peclet number directly from its definition as the ratio of advective to diffusive transport rates, given by $Pe = \delta s/\sqrt{4/\pi D \delta t}$. The time duration of a single jump is determined as $\delta t = \delta s/v$, where v is the magnitude of the fluid velocity at the current particle location. Assuming that the change in the mean conductivity value is minor over the

simulation time, we can replace v with the initial flow velocity $v_0 = K_0/\theta_0 \cdot \Delta h/L$. Thus, we finally obtain the expression for the Lagrangian transport Peclet number in our simulation

$$Pe = \sqrt{\frac{\pi \delta s \, K_0 \, \Delta h_{BC}}{4 \, D \, L_x \, \theta_0}} \tag{11}$$

The above definition provides a direct estimate of the relative contributions of the advective and diffusive processes in the transport in porous media. This approach may prove useful for Lagrange particle tracking methods where the advective and diffusive transport contributions are defined explicitly.

To investigate the influence of the Peclet number of the transport on the evolution of the reactive process and the emergence of transport self-organization in the field, we simulate a number of reactive transport scenarios for different values of the Peclet number. This is achieved by applying different values of the inlet-outlet hydraulic head drop boundary condition Δh_{BC}. The computational time step Δt is correlated with Δh_{BC} in such a way that in each simulated reactive transport scenario, corresponding to a specific value of applied Δh_{BC}, an equal number of 1800 time steps Δt and, correspondingly, reaction events occur per pore volume time T_{pv}.

3 Identifying and quantifying self-organization

3.1 Emergence of transport self-organization in reactive transport in an initially homogeneous porous media

The computational setting described in the previous section mimics the dynamics of a coupled dissolution-precipitation reactive process in a calcite porous medium, leading to an emergence of heterogeneity in an initially homogeneous field. Previous studies have shown that self-organization of the solute transport in the field is expected to emerge in such a situation in the form of preferential flow paths that lead to solute concentration gradients in the direction transverse to flow [Zehe et al. (2021)], yet the details of this self-organization emergence and evolution are critical to understanding the large-scale dynamics of the coupled reactive process in the field. To analyze the emergence of self-organization in our computational field, we consider snapshots of the field in terms of hydraulic conductivity distribution, taken at different computational times as the reactive process in the field evolves. We consider each snapshot as an open thermodynamic system and perform a non-reactive tracer test by injecting non-reactive solute at the field's inlet. Along the lines of Section 1.2, we argue that organized states, characterized by reduced entropy, can emerge in an open system, driven away from equilibrium due to exchange of energy or matter with surroundings. Such a system may persist in a stationary nonequilibrium state. Since, according to the second law, overall entropy cannot decrease, in such a case entropy must be exported from the system outside, leading to an increase in the entropy of its surroundings.

Appendix A in the Supplementary data presents a simple heat transfer example that illustrates how an open thermodynamic system can be maintained in a stationary nonequilibrium state through an inflow of energy. Following the same concept, one

can generalize this finding for the system under investigation, represented by a snapshot of the reactive field at a specific computational time, where the non-reactive solute transport self-organization in the field in terms of emergence of preferential flow paths is the outcome of the coupled reactive process that introduces heterogeneity in an initially homogeneous field. In our system, energy influx occurs in the form of hydraulic power, supplied to the flow to overcome the hydraulic resistance of the field by the applied hydraulic pressure head drop boundary condition Δh_{BC}. Such a system may persist in a nonequilibrium stationary state, characterized by the lowered entropy of the transversal distribution of solute concentration, with the hydraulic power, supplied to the flow, acting against depletion of transversal concentration gradients. For our system, an equilibrium state corresponds to the state of perfect mixing in the field, where no such gradients exist [Zehe et al. (2021)].

To identify the driving mechanism that leads to an emergence of heterogeneity in an initially homogeneous porous medium, followed by self-organization of the solute transport in the field, let us consider two limiting cases related to the nature of the transport mechanism in the field, as applicable to our reactive transport setting, described in Section 2. First, we consider a case when no advection is present (the advective velocity $v = 0$). In this scenario, reactive A particles advance within the field due to diffusive action only. Because of the stochastic nature of the diffusive process that lacks spatial preference, and since the diffusive properties of the reactant and the product particles are identical (also, in our model diffusion is independent of porosity), we expect that the dissolution and precipitation reactions will occur uniformly in space, thus the conductivity field will remain approximately homogeneous in the direction transverse to flow. Therefore, we suggest that in the absence of advection no mechanism exists in our reactive setup to create heterogeneity in the field and no transport self-organization will take place in that case. In the opposite limiting case when no diffusion is present (the diffusion coefficient $D = 0$), a dissolution reaction will first take place uniformly at the inlet of the initially homogeneous field as the reactive A particles enter the field. The resulting carbonic acid particles, in accordance with the reaction equation (3), will be swept downstream by the advective flow to cause precipitation reaction uniformly along the direction transverse to flow at some distance downstream. This pattern of alternating dissolution and precipitation areas at identical intervals in the downstream direction will repeat itself, the resulting pattern being reminiscent of a precipitation banding phenomenon [Singurindy and Berkowitz (2003)]. Again, in this case no heterogeneity in the direction transverse to flow is expected to emerge, thus we suggest that no transport self-organization will occur as well.

Following the above discussion, we argue that for the transport self-organization to emerge in an initially homogeneous field undergoing a dissolution/precipitation reactive process as defined in our reactive setup, it is necessary for the transport mechanism to include both diffusive and advective contributions. Here, the stochastic diffusion leads to local concentration variations in H^+, that in turn create local variations in hydraulic conductivity, while the advection follows these conductivity variations, funneling the flow towards the higher conductivity areas and further increasing their conductivity due to the enhanced dissolution by the funneled A particles. This creates positive coupling between the reactive and transport processes. Here, an analogy can be made to the Turing's morphogenesis model (see Section 1.2), where the homogenizing action of the diffusion is counteracted by the fact that the diffusion coefficients of the reacting substances differ, which is a prerequisite for the appearance

of self-organizing patterns. We suggest that the driving force for transport self-organization in the model under investigation is the ratio between the diffusive and advective transport rates, or the reciprocal of the Peclet number. Therefore, we expect to obtain an increase in transport self-organization in the field with a decrease in the Peclet number of the flow.

In an attempt to derive an analytical justification for this, let us relate the heterogeneity, emerging in an initially homogeneous field due to the coupled reactive-transport process, to the global reaction rate in the field. The reasoning behind this is that in the initially homogeneous field, reaction that occurs in the field is the driving force behind the emergence of heterogeneity there; heterogeneity, in turn, is responsible for the emergence of transport self-organization in the field. While some of the reaction events that occur may cancel each other out in terms of dissipating or precipitating some of the calcite in a computational cell, the remaining part of reaction is "useful" in creating heterogeneity. Thus, we may speculate that the reaction rate and the emergence of heterogeneity in the field are directly related. Consider, for simplicity, a 1D Advection-diffusion-reaction equation (ADRE)

$$\frac{\partial c}{\partial t} = -v\frac{\partial c}{\partial x} + D\frac{\partial^2 c}{\partial x^2} - G/\theta \tag{12}$$

where c is the solute concentration, v is the advective velocity, D is the diffusion coefficient, G is the reactive term and θ is the porosity of the medium. Let us consider a simple scenario of adsorption / desorption reaction, for which parallels can be drawn to the dissolution / precipitation scenario in our study [Raveh-Rubin et al. (2015)]. A simplest case would be to employ a linear case of the Freundlich isotherm model, where the adsorption is directly proportional to the concentration (see Berkowitz et al. (2014) and Bear and Cheng (2010))

$$A = k_d c \tag{13}$$

where A is the amount of adsorption and k_d is the distribution (sorption) coefficient. For desorption, the sign of the reaction term should be reversed. The reactive term G obtains the following shape

$$G = \rho_b\frac{\partial A}{\partial t} = k_d\rho_b\frac{\partial c}{\partial t} \tag{14}$$

where ρ_b is the dry bulk density of the porous medium. After some manipulation, the ADRE for the adsorption case may be written as

$$R\frac{\partial c}{\partial t} = -v\frac{\partial c}{\partial x} + D\frac{\partial^2 c}{\partial x^2} \tag{15}$$

where $R = 1 + k_d\frac{\rho_b}{\theta}$ is the retardation factor. To obtain the non-dimensionalized version of ADRE, we normalize all variables as follows: $\tilde{c} = c/c_{ref}$ where c_{ref} is the reference value for the solute concentration, $\tilde{x} = x/L_x$ and $\tilde{v} = v/v_0$. The temporal coordinate is normalized by the pore volume time T_{pv} to obtain $\tilde{t} = t\,v_0/L_x$. Thus, the resulting non-dimensionalized version of ADRE is

$$R\frac{\partial\tilde{c}}{\partial\tilde{t}} = -\tilde{v}\frac{\partial\tilde{c}}{\partial\tilde{x}} + \frac{1}{Pe}\frac{\partial^2\tilde{c}}{\partial\tilde{x}^2} \tag{16}$$

where $Pe = L_x v_0/D$ is the classical definition of the Peclet number. Recalling the linear relation between the adsorption and the concentration (13), we may write for the non-dimensional adsorption rate

$$\frac{\partial \tilde{A}}{\partial \tilde{t}} = \frac{k_d c_{ref}}{R A_{ref}} \left(-\tilde{v} \frac{\partial \tilde{c}}{\partial \tilde{x}} + \frac{1}{Pe} \frac{\partial^2 \tilde{c}}{\partial \tilde{x}^2} \right) \tag{17}$$

where $\tilde{A} = A/A_{ref}$, A_{ref} being the reference value for the adsorption amount. To obtain the global reaction rate in the field, (17) should be integrated over the domain. For the case when the advective transport contribution is small relative to the diffusive one $\left(-\tilde{v} \frac{\partial \tilde{c}}{\partial \tilde{x}} \ll \frac{1}{Pe} \frac{\partial^2 \tilde{c}}{\partial \tilde{x}^2} \right)$, this result suggests the dependence of the global reaction rate on the reciprocal of Peclet for our simple model. Recalling an assumption made earlier about the heterogeneity and, thus, the ensuing transport self-organization in the field being directly related to the global reaction rate, we arrive at a conclusion that both these parameters depend on the the reciprocal of the Peclet number for diffusion-dominated flows.

3.2 Self-organization quantization employing Shannon entropy

Having obtained a qualitative understanding of the subject of self-organization in the context of reactive transport of the porous medium, we shall now seek for a way to characterize this phenomenon quantitatively using a concept of Shannon entropy, also referred to as "information entropy". Shannon entropy was introduced originally in the field of communication theory, whose fundamental problem is formulated as "*reproducing at one point either exactly or approximately a message, selected at another point.*" [Shannon (1948)]. Viewing communication as a statistical process, Shannon employed an entropy-like parameter to provide a measure for the amount of transmitted information, carried by a certain sequence of symbols (a message). Appendix B in the Supplementary data contains a short account of the Shannon entropy, while here we only reprint the main result

$$S = -\Sigma_i \, p_i \log_2 p_i \tag{18}$$

where S is the Shannon entropy per symbol of the message and $p_i = n_i/n$, $i = 1...N_s$ are the relative occurrence frequencies of N_s different symbols that constitute the message, calculated as a ratio of the number of occurrences of a specific symbol i in the message n_i to the total message length n.

The definition of information entropy, given by Shannon, is equivalent to physical entropy in statistical mechanics as defined by Gibbs, where the logarithm in (18) is to the base of e and the sum is multiplied by the Boltzmann constant [Ben-Naim (2008)]. The statistical definition of a physical entropy characterizes the number of possible microstates of a system that are consistent with its macroscopic thermodynamic properties which constitute the macrostate of the system. Thus, in case of a gas consisting of a large number of molecules in a container, a microstate of the system consists of position and momentum of each molecule, as it moves within the container, colliding with other molecules and container walls. A multitude of such microstates correspond to a single macroscopic state of the system, defined by its pressure and temperature. The parameter p_i in this case corresponds to a probability that a microstate i occurs during the system's fluctuations. According to the second law of Thermodynamics, entropy of a system reaches its maximum value at equilibrium, where gradients of thermodynamic

parameters are depleted by dissipative forces and the measure of order in the system is at its minimum. In this case, each microstate is equally likely and p_i is simply the inverse of the total number of microstates (Kondepudi and Prigogine, 1998).

450   To characterize the emergence and development of transport self-organization in an initially homogeneous field as the dissolution-precipitation reactive processes in the field evolve, we adopt a straightforward use of the Shannon entropy, in a similar vein to Zehe et al. (2021), where it was employed in the context of characterizing self-organization in heterogeneous non-reactive groundwater systems. In order to place all results on equal footing, we perform additional computational *non-reactive* tracer tests on the snapshots of the hydraulic conductivity field at different simulation times, as described in Section 3.1. The non-

455   reactive particle tracer algorithm, employed for this purpose, consists of the flow and particle transport algorithm as described in Section 2.2, but without the kinetic reaction part. A total number of $N_{tot}^{NR} = 1e5$ particles, that represent the non-reactive tracer solute (not to confuse with the number of reactive particles N_{tot} injected per T_{pv} in the reactive algorithm), are injected at the inlet of the computational field, subject to identical hydraulic pressure head drop boundary condition of $\Delta h_{BC} = 100cm$, and allowed to advance within the field subject to laws described in Section 2.2, until all of them reach the outlet boundary. The

460   relatively large value of Δh_{BC} is chosen in order to eliminate the diffusive transport contribution which tends to smooth out concentration gradients due to its stochastic character. The injected particles are flux-weighted according to the conductivity distribution of the inlet cells. The field density matrix, obtained by counting the total number of particle visitations in each computational cell, is saved for each field snapshot. From this matrix, the solute concentration distribution of the non-reactive tracer across the field is obtained. We recall the proposition put forth by Berkowitz and Zehe (2020) that solute transport self-

465   organization corresponds to an emergence of solute transport gradients in the field in the direction transverse to the direction of the flow. To quantify the entropy of transport self-organization in the snapshots of the hydraulic conductivity field, we rewrite (18) as follows

$$S(x) = -\Sigma_i p_i \log_2 p_i \tag{19}$$

where $S(x)$ is the Shannon entropy of the transversal solute concentration at a given axial coordinate x and $p_i = N_i/N_{tot}^{NR}$, $i = $

470   $1...N_y$ is the relative solute concentration distribution at x in the direction transverse to flow (here, N_i is the number of particles that have passed through the i-th cell at x).

3.3   The relation between self-organization, heterogeneity and hydraulic power

Following the thermodynamic framework, as applied to the system under investigation, energy must be invested in the heterogeneous field to maintain an ordered state of solute transport there. This energy comes in the form of hydraulic power that

475   enables the flow to overcome the hydraulic resistance of the porous medium under the applied hydraulic pressure head drop boundary condition Δh_{BC}. The total hydraulic power dissipated by the flow while overcoming the hydraulic resistance of the field is an extensive parameter and is given by a cell-wise summation

$$P_{total} = -\rho_f g \sum_{i,j} \Delta h_{ij} \cdot Q_{ij} \tag{20}$$

where i, j are the row and the column indices of the (i,j)-th cell in the field, respectively, Δh_{ij} and Q_{ij} are the hydraulic head drop and the volumetric flow rate through the (i,j)-th cell, ρ_f is the fluid density and g is the gravitational acceleration.

In an attempt to better understand the relation between the degree of heterogeneity of the porous medium and the hydraulic power required for the fluid to overcome the resistance of the medium under the inlet-outlet hydraulic head drop boundary condition Δh_{BC}, we consider a simplified model of the field as a series of conductive channels connected in parallel. These channels have no interaction transversally, and the deviations of their shape from the shortest path between the inlet and the outlet (a straight line) is not significant. This model corresponds to a moderately heterogeneous field that consists of a number of preferential flow paths where most of the solute transport (and, thus, most of the reaction) occurs. Assuming that the heterogeneity introduced into the field due to the coupled reactive-transport process is minor, the shape of the obtained preferential flow paths indeed should not stray too far from a straight line. Each conductive channel is represented by a collection of cells along the preferential flow path in the field. The equivalent hydraulic conductivity of the i-th single channel is

$$K_i^{EQ} = L_i / \underset{j}{\Sigma} \Delta l_j \cdot K_{ij}^{-1} \qquad (21)$$

where the index j runs along the cells that constitute the i-th channel, L_i is the total length of the channel and K_{ij}, Δl_j are the hydraulic conductivity and the length of the preferential path segment inside the j-th cell of the i-th channel (do not confuse with the row and column indices i, j as defined earlier. For the most general case of a curvilinear flow path the i, j indices may not conform to the row and column indices). The equivalent hydraulic conductivity of the whole field, viewed as a system of conductive channels, connected in parallel, is

$$K_{field}^{EQ} = \sum_i K_i^{EQ} \cdot \frac{\Delta y}{L_y} = \frac{\Delta y}{L_y} \sum_i \frac{L_i}{\underset{j}{\Sigma} \Delta l_j \cdot K_{ij}^{-1}} \qquad (22)$$

Under the assumption of parallel channels with no interaction taking place between them transversally, the total hydraulic power dissipated in the field is given by:

$$P_{total}^{EQ} = -\rho g \Delta h_{BC} \cdot Q_{total} = \rho g \left(\frac{\Delta h_{BC}}{L_x}\right)^2 L_x L_y K_{field}^{EQ} \qquad (23)$$

where Q_{total} is the total volumetric flow rate through the field. To relate the increase in hydraulic power with an emergence of heterogeneity in the field, which leads to the increasing transport self-organization, consider again the relations (22) and (23) given above. The total hydraulic power in the field, calculated using the parallel channels assumption P_{total}^{EQ}, is related to the hydraulic conductivity distribution by virtue of the equivalent hydraulic conductivity of the field (22), which can be rewritten as

$$K_{field}^{EQ} = \frac{\Delta y}{L_y} \sum_i \frac{1}{R_i} \qquad (24)$$

where $R_i = (1/L_i)\underset{j}{\sum} \Delta l_j \cdot K_{ij}^{-1}$ is the reciprocal of the equivalent hydraulic conductivity of the i-th channel K_i^{EQ}, or its hydraulic resistivity. Recall the well-known feature of the harmonic mean of some population: if the population is subjected to a

mean-preserving spread (that is, its variance is increased while the mean is kept at a constant value), then its harmonic mean always decreases [Douglas, 2004]. Since (24) can be viewed as a reciprocal of harmonic mean of the population of hydraulic channel resistivities R, we expect that K_{field}^{EQ} will increase with an increase in the variance of R, assuming the change in the mean hydraulic conductivity of the field is minor. Moreover. since the variance of R depends directly on the variance of the hydraulic conductivity distribution K in the field, it is reasonable to expect that K_{field}^{EQ} will increase with an increase in the variance of K, which signifies the emergence of heterogeneity in the initially homogeneous field. Thus, an increase in heterogeneity of an initially homogeneous porous medium due to the coupled reactive process requires an increase in the hydraulic power, supplied to the flow to overcome the hydraulic resistance of the medium under the maintained hydraulic head drop boundary condition Δh_{BC}, applied to the field. Within the adopted thermodynamic framework, this increase in power allows to increase the spatial self-organization of the solute transport in the field. To conclude, the increase in the hydraulic power, dissipated in the field, as well as the emergence of transport self-organization, are both the result of an increase in the heterogeneity of the field. The latter, in turn, can be viewed as a consequence of the energy invested in the field by the dissolution / precipitation reactive process.

We emphasize that the presented study does not intend to construct a complete thermodynamic formalism for the problem under investigation, such as the one that is presented in Hansen et al. (2018) and Hansen et al. (2023). The thermodynamic framework presented in the current study is aimed at providing qualitative dependencies / trends between the parameters of interest, such as the entropy of the transport self-organization, the hydraulic power, dissipated in the field, etc. It is our intent to arrive at a more complete thermodynamic formalism for the reactive flow in porous medium in the course of the research work.

4   Results and discussion

Based on the reactive transport algorithm described in Section 2, we analyze the evolution of the reactive process in an initially homogeneous reactive field and demonstrate that the parameters that characterize this evolution, such as global reaction rate, mean value and variance of the hydraulic conductivity distribution, indeed depend on the reciprocal of Peclet, as suggested by the analytic result derived in Section 3.1. We then investigate the emergence and evolution of transport self-organization in the field along with the advancement of the reactive process, and showcase that transport self-organization correlates with the reciprocal of the Peclet number as well. To investigate these relations, we simulate a number of reactive transport scenarios for different values of the ratio of advective to diffusive transport rates, characterized by the Peclet number, calculated as shown in Section 2.4. This is achieved by applying different values of the inlet-outlet hydraulic pressure head boundary condition Δh, as described therein. Thus, for Δh = 1e-4, 1e-3, 1e-2 and 1e-1[cm], we obtain the Peclet number to be approximately Pe = 0.38, 1.2, 3.8 and 12.0. A reaction enhancement by a factor of 5e2 is employed (see Section 2.3). We follow this series of analyses by quantifying the evolution of transport self organization in time as described in Section 3.2, showing that transport self-organization in the field increases with a decrease in the Peclet number, as expressed by the reduction in the Shannon entropy.

The self-organization of the breakthrough curve exhibits the opposite tendencies, that are ~~explained from the thermodynamic perspective~~ observed from the perspective of a thermodynamic analogy. The hydraulic power, required to maintain the driving head pressure drop boundary condition between inlet and outlet, increases with the increasing variance ~~, as well as with the mean value,~~ of the hydraulic conductivity distribution in the field, as suggested by the simple parallel channels model, developed in Section 3.3 (along with the contribution of the mean value of conductivity). This increase in power results in an increase in the transport self-organization in the field.

4.1 Evolution of reactive process in the field

We begin by examining the evolution of the reactive process, as depicted by the snapshots of the relative hydraulic conductivity $K - K_0$ of the field at different normalized times $\tilde{t} = t/T_{pv}$, shown in Figures 1a–c (obtained from a realization of the reactive process for $Pe = 0.38$). The normalized time $\tilde{t}$ is defined in such a way that for $\tilde{t} = 1.0$ the reactive front has permeated through the whole media. As the reactive particles advance and react in the initially homogeneous field, heterogeneity is being introduced into the field in the form of local dissolution and precipitation areas, signified by positive and negative values of $K - K_0$, respectively. This heterogeneity advances downstream alongside the reactive particles, with the local dissolution / precipitation areas intensifying with time as the reactive process in the field develops, creating a clearly distinguishable reaction front. Downstream of the front, the field remains homogeneous as the reactive process hasn't arrived there yet. A dissolution area is located In the immediate vicinity of the inlet, where the chemical equilibrium is tilted towards dissolution; this correlates with experimental and simulation observations [Poonoosamy et al. (2020), Deng et al. (2022)]. The correlation length of these field snapshots was found to be of the order of the size of the computational cell, therefore no larger structures in the hydraulic conductivity distribution are observed.

The influence of the Peclet number on the evolution of reactive process in the field is characterized in Figures 2a–d. Figure 2a presents the global reaction rate $\dot{R}$, which was calculated as the mean value of the absolute rate of change of hydraulic conductivity with dimensionless time $|dk/d\tilde{t}|$ over all computational cells, as a function of dimensionless time $\tilde{t}$. This parameter takes into an account the overall amount of "useful" reaction that takes place, including both dissolution and precipitation. Here, the term "useful" is applied to reaction events that didn't cancel each other, but served to alter the hydraulic conductivity distribution in the field. The calculation was performed excluding the area of 10 computational cells in the immediate vicinity of the inlet, so to focus on the evolution of the reactive process within the field, excluding the inlet conductivity alteration, where the reactive process is tilted towards dissolution; this effect is of a very localized nature and, thus, was ignored. We observe that the global reaction rate increases with dimensionless time in a linear fashion, as the reactive particles sample more of the field's territory at an approximately constant mean velocity, which allows broader opportunities for reaction. Beginning from $\tilde{t} = 1$, $\dot{R}$ becomes approximately constant, as the reactive particles have sampled an entire field at that point. The influence of the Peclet number is clearly exhibited by the fact that the global reaction rate increases with the reciprocal of Peclet, showing that diffusive transport mechanism, responsible for mixing in the field, enhances the reactive process. This can be explained by the fact that diffusion, being stochastic in nature, allows particles to sample regions also in the transverse direction, away
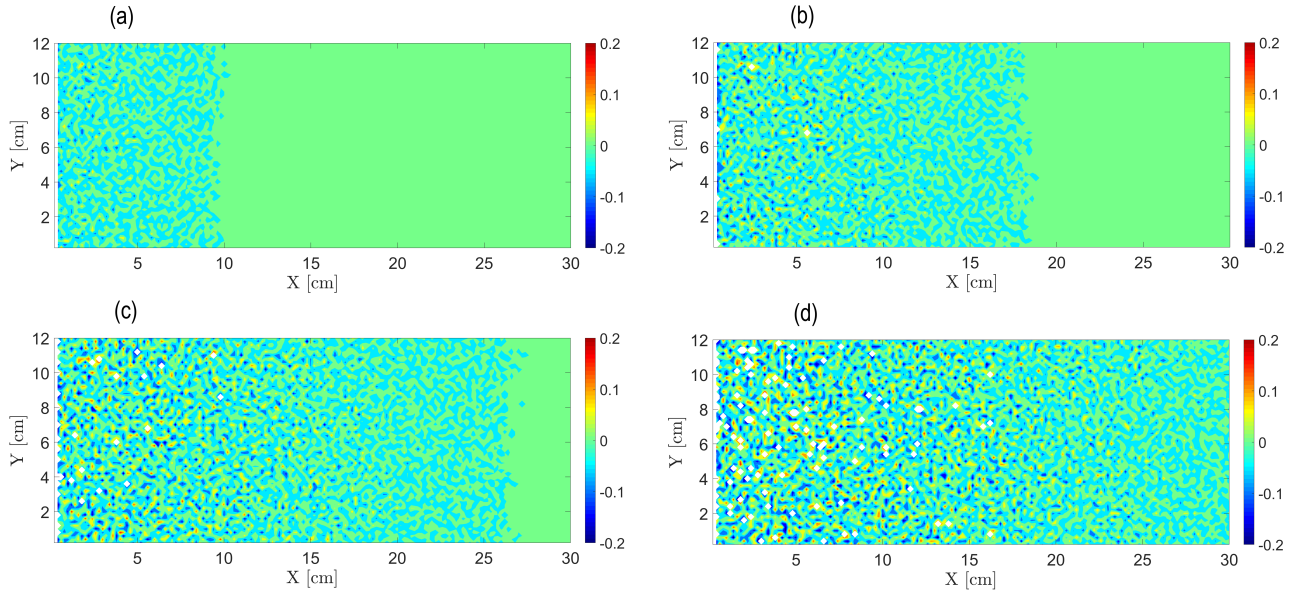
Figure 1. Evolution of the relative hydraulic conductivity $K - K_0 \, [\text{cm} \, \text{min}^{-1}]$ field over time for Pe = 0.38: (a) $\tilde{t} = 0.25$, (b) $\tilde{t} = 0.5$, (c) $\tilde{t} = 0.75$ and (d) $\tilde{t} = 1.0$.

from the path suggested by the advection mechanism, which allows a better chance for reaction. This result further confirms the findings of [Nissan and Berkowitz (2019)] on bimolecular reaction, where an increase in the reactant production rate with a decrease in Peclet was reported, due to an increase in the spatial spread of the transported species; this trend was also reported in Edery et al. (2021).

580

To verify the dependency of the global reaction rate on the reciprocal of Peclet, as suggested by the theoretical result obtained in Section 3.1, the scalability of the curves in Figure 2a with the Peclet number was investigated. Assuming separation of variables in $\dot{R}$, so that $\dot{R} = f(\tilde{t}) \cdot g(Pe)$ and the Peclet dependency takes on the form of $g(Pe) = a \cdot Pe^{-1} + b$, satisfying results were obtained for $a, b = 3.403, 3.984$ ($R^2 = 0.994$). The scaled curves, obtained by dividing the computed curves by

585 the estimated $g(Pe)$, are depicted in the figure inset. The relation (17) also suggests the reason as to why at higher Peclet numbers the Peclet dependency diminishes, and the global reaction rate approaches an approximately constant (independent of Peclet) non-zero value. Similarity solutions $\tilde{c} = f(\tilde{x}, \tilde{t}, Pe)$ for (17) are possible if the normalized velocity $\tilde{v}$ remains identical in the different Peclet number scenarios. In case of a minor transport-reaction interaction that leads to minor conductivity changes, the deviations in the velocity field from the initial value can be assumed minor as well, thus $\tilde{v} \approx 1$. For high Peclet

590 values, the similarity solution to (17) is approximately Peclet-independent. ~~Indeed, as~~ As follows from Figure 2a, the ratio between the global reaction rate for $Pe = 12$ and $Pe = 0.38$ is about 4, which may hint at the fact that the advective contribution to reaction rate is small compared to the diffusive contribution for the lower range of Peclet numbers in the current study.

Figure 2b presents the normalized global reaction rate $\dot{R}_{norm}$, that was obtained by normalizing the global reaction rate $\dot{R}$ by the distance from inlet sampled by the flow $L_x \tilde{t}$ (excluding the area in the vicinity of the inlet). This was done in order to obtain an indication of the reaction rate per unit area where the reaction takes place. After the transitional effects fade, $\dot{R}_{norm}$ exhibits an approximately constant behavior, as expected. Recall that on a local scale in our model the reaction is instantaneous [Edery et al. (2021)]. Here, as well, the scalability with the reciprocal of Peclet exists, taking the same form as in the case of the non-normalized global reaction rate $\dot{R}$. The scaled curves are depicted in the figure inset.

Figure 2c presents the deviation of the mean value of hydraulic conductivity over all computational cells from the initial conductivity $\tilde{K} - K_0$ as a function of dimensionless time $\tilde{t}$. Here, the area of 10 computational cells in the immediate vicinity of the inlet was excluded from the calculation as well. Clearly, the net reaction is tilted towards dissolution, as $\tilde{K} - K_0$ grows monotonously with $\tilde{t}$, which is reasonable due to the influx of low pH fluid at the inlet of the field (see also Edery et al. (2021)); the relative increase in hydraulic conductivity is small comparing to K_0. This result is in agreement with the findings of Edery et al. (2021). The power law shape holds well, beginning with approximately $\tilde{t} = 0.3$. The onset of the power law region coincides with the time when a large enough particle ensemble has reacted within the field to create a statistically consistent picture. The curves for larger Peclet numbers exhibit fluctuations for the considerable portion of time, however they comply with the power law shape eventually as well. $\tilde{K} - K_0$ also increases with the decrease of the Peclet number, again due to the reaction enhancing role of the diffusive transport mechanism. Here, as well, the scalability with the reciprocal of Peclet exists. Assuming again separation of variables as before, so that the Peclet dependency takes on the form $g(Pe) = a \cdot Pe^{-1}$, good results were obtained for $a = 0.007624$ ($R^2 = 0.985$). This can be justified by again relating the parameters that govern the evolution of the reactive process in the field to the reaction rate, for which the Peclet dependence was shown to have the same shape. All Peclet-scalability related conclusions drawn for Figure 2a are applicable here as well. The scaled curves are depicted in the figure inset.

Similar trends are observed in Figure 2d, that presents the variance of hydraulic conductivity σ_k^2 as a function of dimensionless time $\tilde{t}$. Here, the area of 10 computational cells in the immediate vicinity of the inlet was excluded from the calculation as well. This parameter, being the measure of the field's heterogeneity, is indicated as the primary cause for transport self-organization in the field [Zehe et al. (2021)]. σ_k^2 increases monotonously with dimensionless time $\tilde{t}$, as the particles sample more field regions and react at an increasing rate, this result again being in agreement with the findings of Edery et al. (2021). Heterogeneity also increases with the decrease of the Peclet number, again due to the reaction enhancing role of the diffusive transport mechanism. We thus state that reactive transport scenarios with lower values of the Peclet number, corresponding to dominant diffusive transport mechanism, coincide with an increased reaction rate in the field and, thus, increased field's heterogeneity. The power law shape holds well for all Peclet cases, beginning with approximately $\tilde{t} = 0.2$. Turning again to the findings of Edery et al. (2021), where the coupled reactive process was investigated within the framework of the continuous time random walk (CTRW) approach, we emphasize the anomalous (non-Fickian) nature of the ensuing transport, that is traced back to the coupling between the reactive and transport processes in the initially homogeneous field. Here, as well, the scalability with the
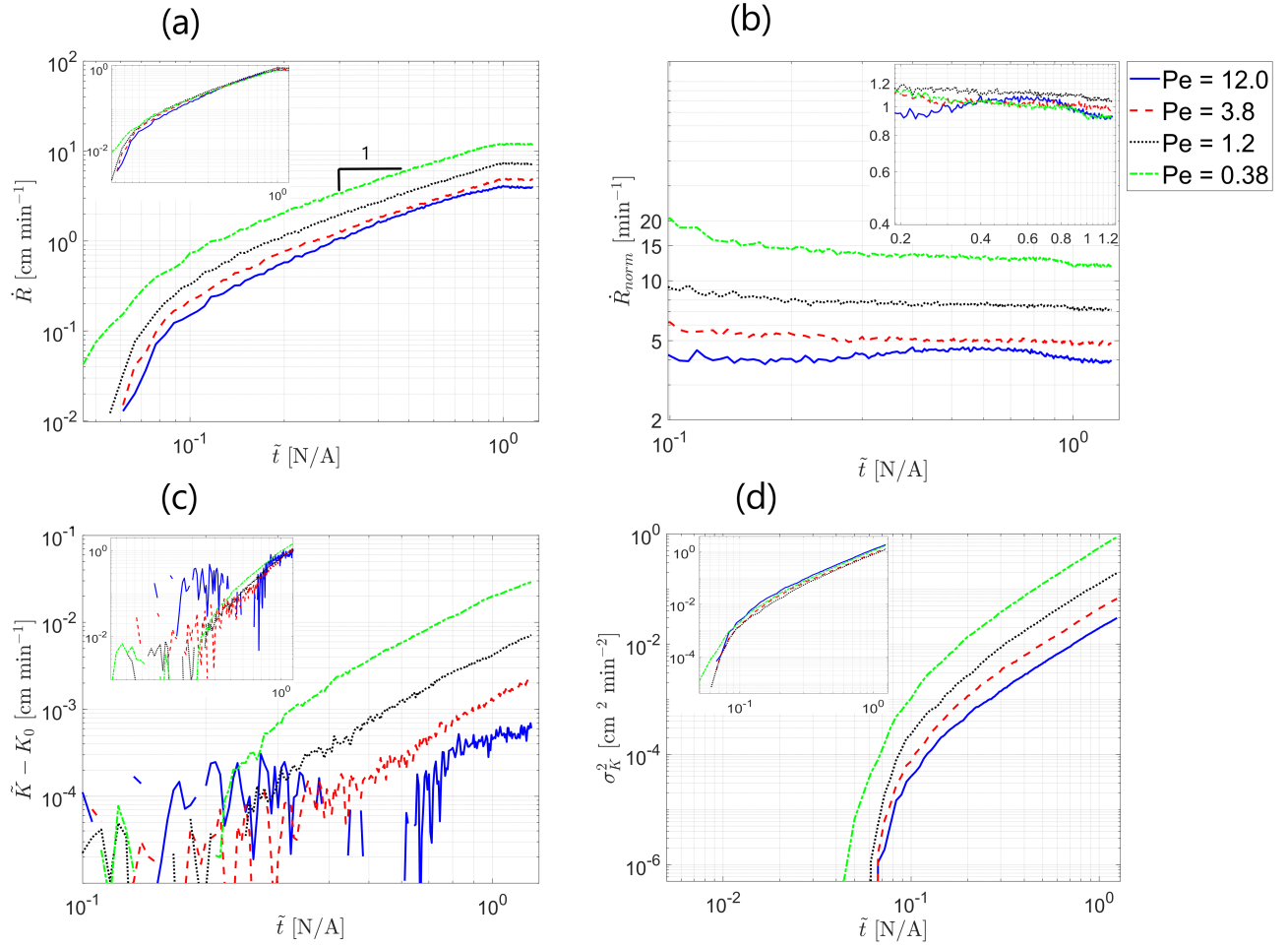
Figure 2. influence of Peclet number on the evolution of the reactive process in the field over time: (a) Global reaction rate $\dot{R}$, (b) Normalized global reaction rate $\dot{R}_{norm}$, (c) Deviation of the mean hydraulic conductivity from initial value $\tilde{K} - K_0$ and (d) Hydraulic conductivity variance σ_k^2, as a function of dimensionless time $\tilde{t}$. Insets show Peclet-scaled curves, obtained by assuming a power-law Peclet dependency (a dependency on the reciprocal of Peclet was obtained for all displayed parameters, as an exponent value of -1 resulted in a satisfying fit for all curves).

reciprocal of Peclet exists. Assuming again separation of variables as before, so that the Peclet dependency takes on the form $g(Pe) = a \cdot Pe^{-1}$, good results were obtained for $a = 0.001616$ ($R^2 = 0.987$). All Peclet-scalability related conclusions drawn for Figures 2a–c are applicable here as well. The scaled curves are depicted in the figure inset.

The dependence of the parameters, depicted in Figures 2a–d, on the reciprocal of the Peclet number confirms that this dimensionless number is indeed the driving force behind the evolution of the reactive process in the field. The fact that Peclet-related tendencies, obtained in Section 3.1 for the simple one-dimensional ADRE scenario with an adsorption reaction case, represented by the linear Freundlich isotherm, have been verified in the Lagrangian particle tracker numerical simulations presented above, where a considerably more complex reversible reaction of dissolution / precipitation of calcite is considered, suggests a general validity of these tendencies for the case of minor heterogeneity variations that lead to minor fluctuations in concentration. An important note should be made regarding the initial state of the field that undergoes reactive process: in our case of an initially homogeneous field, diffusion acts as an enhancing factor for the emergence of heterogeneity in the field; in an initially heterogeneous case, such as in [Al-Khulaifi et al. (2017)], diffusion is capable of decreasing the heterogeneity of the porous medium due to its smoothing property.

The relatively small scale of the phenomenon presented in this study must be pointed out. The initial state of the porous medium is completely homogeneous, and the heterogeneity that develops is relatively minor. The trends presented could have been more pronounced quantitatively, had the simulation been allowed to run longer. The simulation was stopped soon after pore volume time was reached due to computational time limitations, since running the LPT code with large number of particles consumes considerable computational resources. Had the model been allowed to run longer, the mean conductivity and the heterogeneity trends are expected to further increase, while the dependency of the reactive transport evolution on the reciprocal of Peclet is expected to persist as long as the degree of heterogeneity of the field remains moderate (see Section 3.1).

4.2 Transport self-organization in the field

To characterize the emergence and development of transport self-organization in our model as the dissolution-precipitation reactive processes in the field advance, we adopt a straightforward use of the Shannon entropy, similar to Zehe et al. (2021), where it was employed in the context of characterizing self-organization in non-reactive flows in heterogeneous groundwater systems. In order to place all results on equal footing, we perform computational *non-reactive* tracer tests on the snapshots of the hydraulic conductivity field at different values of the dimensionless time $\tilde{t}$, as described in Section 3.2.

The emergence of transport self-organization in the reacting field is evident from the Figures 3a-d that present the decimal logarithm of the relative non-reactive tracer concentration $\tilde{c}$ in the snapshots of the field that undergoes reactive process at $Pe = 0.38$, for different values of the dimensionless time $\tilde{t}$. $\tilde{c}$ is defined as the ratio of the total number of non-reactive particle visitations in a cell to the number of particle visitations in a cell in the equilibrium state (represented by perfect mixing in the field) Here, the number of particle visitations in the equilibrium state is defined by N_{tot}^{NR}/Ny, which corresponds to

the case of a uniform particle injection in the completely homogeneous field, where the same number of particles visits each cell in the field. This parameter is analogous to the non-reactive solute relative concentration obtained from the tracer tests. With the passage of time, variations in the hydraulic conductivity of the field due to the reactive process create autocatalytic feedback mechanism that leads to an emergence of finger-like preferential flow paths. These paths interact, competing for the available flow, so that eventually some of the paths carry a significantly larger part of the injected particles than the others, as seen from the increasing concentration gradients in the direction transverse to flow. This can be explained by observing the mechanism responsible for transport self-organization in the field. The particles injected at the inlet of the field are being flux-weighted, meaning that the number of particles injected in each of the inlet cells is proportional to Darcy flux in that cell. Diffusion, treated as a stochastic agent in our model, leads to appearance of hydraulic conductivity fluctuations in the initially homogeneous field in the direction transverse to flow. Thus, the more conductive paths receive more Darcy flux, which in turn attracts more reactive A particles to them, making these paths even more conductive. This autocatalytic process leads to constant intensification of this phenomenon, as shown in Figures 3a-d. The observed flow paths are linear in shape, with negligible tortuosity, due to the hydraulic conductivity deviations from the initial value being minor. Another reason for this is that the correlation length of the produced heterogeneous fields is small as well, leading to absence of large-scale structures, that could alter significantly the direction of the preferential flow paths. This picture corresponds to the simplified hydraulic model presented in Section 3.3, where the field was considered as a series of approximately linear conductive channels connected in parallel. The similarities of the simulated scenario to that of reactive infiltration, as reported in Szymczak and Ladd (2006), where a pore-scale numerical model was used to investigate channel growth and interaction due to dissolution in fractures, have to be pointed out. Their model employed Lattice-Boltzmann method for flow field calculation, while the transport of dissolved species was modeled by a random walk algorithm that efficiently incorporates the chemical kinetics at the solid surfaces. They reported the emergence of a solid-fluid interface instability, with undulation areas formed first at the solid-fluid interface of the porous media due to dissolution, which are later transformed into well-defined finger-like channels or wormholes, that rapidly advance into the medium; as dissolution proceeds, these fingers interact, competing for the available flow, and eventually the growth of the shorter ones ceases.

The deviations of the decimal logarithm of the relative non-reactive tracer concentration $\tilde{c}$, shown in Figures 3a-d, from the equilibrium value of 0 represent either the paths where less particles pass relatively to the equilibrium state (negative values of $\tilde{c}$) or the paths where more particles pass relatively to the equilibrium state (positive values of $\tilde{c}$). Considering the temporal evolution of $\tilde{c}$, one clearly sees an intensification of these deviations from the equilibrium value of 0 with time. In Figure 3d ($\tilde{t}$=1.0), there are a few paths that correspond to the decimal logarithm of $\tilde{c} = -0.4$ and below (61 per cent less particles that visited the path than in the case of a completely homogeneous particle distribution in the field), while some of the others correspond to the decimal logarithm of $\tilde{c} = 0.2$ and above (58 per cent more particles that visited the path than in the case of a completely homogeneous particle distribution in the field).

The observations from Figure 3 are confirmed by the plot of the normalized Shannon entropy of the transport in the field
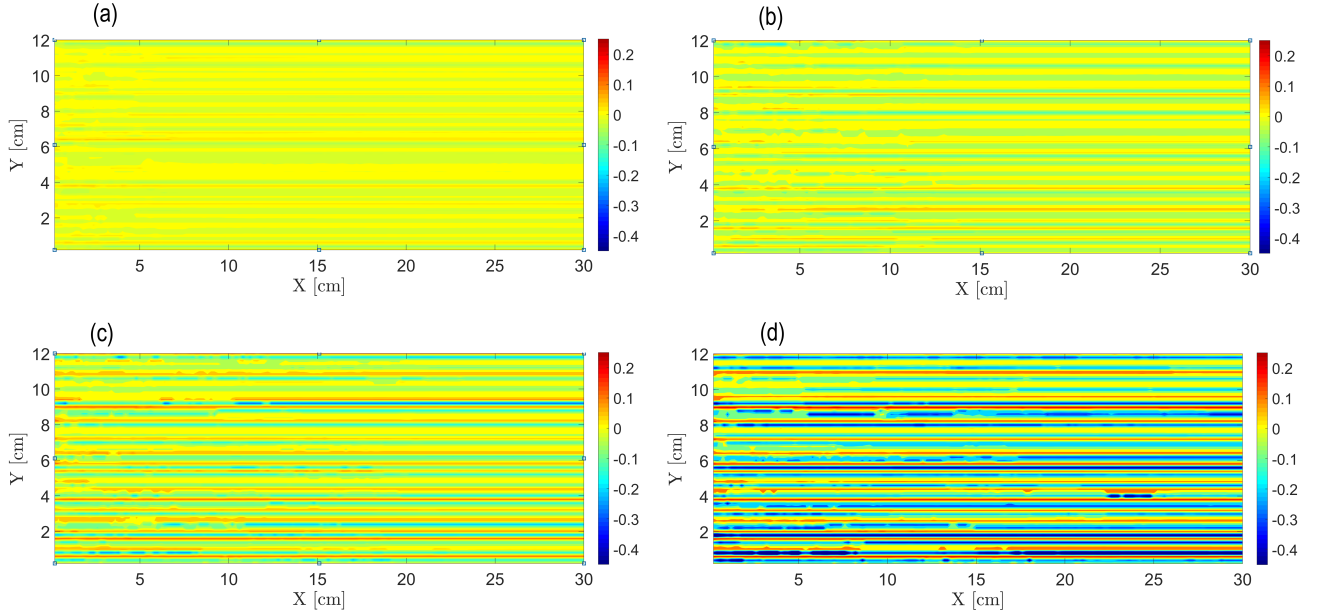
Figure 3. Evolution of the transport self-organization in the field for Pe = 0.38, as represented by the decimal logarithm of the relative non-reactive tracer concentration $\tilde{c}$, based on data obtained from the non-reactive tracer tests performed on the snapshots of the field over time: (a) $\tilde{t} = 0.25$, (b) $\tilde{t} = 0.5$, (c) $\tilde{t} = 0.75$ and (d) $\tilde{t} = 1.0$.

$S_{norm} = (S - S_{max})/S_{max}$ vs. normalized distance from inlet $\tilde{x} = x/L$, calculated from the non-reactive solute concentration data in the snapshots of reactive field at different values of dimensionless time $\tilde{t}$ for $Pe = 0.38$, presented in Figure 4a. Here, S is the Shannon entropy of the transport in the field as a function of the distance from inlet X, calculated from (19) and S_{max} is the maximal possible transport entropy value in the field, calculated as discussed in Section 3.2, so that S_{norm} obtains values from 0 (maximum entropy, no self-organization) to -1 (minimum entropy, maximum self-organization, corresponding to a single preferential flow path channeling all injected solute particles). As the reactive process in the field advances, the resulting level of transport self-organization in the field increases as it reaches further downstream alongside the reaction front, which is signified by the decrease in S_{norm}. Figure 4b presents the mean value of the normalized Shannon entropy of the transport in the field, averaged over the field, $\tilde{S}_{norm}$, vs. dimensionless time $\tilde{t}$ for different values of Peclet number. Again, the plot clearly shows an increase in the transport self-organization in the field with the advance of the reactive process, as the mean normalized entropy $\tilde{S}_{norm}$ decreases over time. A clear picture emerges, where the level of self-organization directly correlates with the Peclet number of the reactive flow, as the normalized entropy $\tilde{S}_{norm}$ decreases with decrease in Peclet. This clearly signifies that diffusive transport mechanism is dominant in initiating transport self-organization in an initially homogeneous field via the coupled reactive process, as it is manifested most significantly for low Peclet numbers that correspond to diffusion-dominated flow. For lower values of the Peclet number, the difference between the neighboring curves is clearly dis-

tinguished, while for larger Peclet numbers, where advection becomes dominant, this difference diminishes, further supporting our discussion on limiting cases for the model under investigation that appears in Section 3.1.

715 In this context, it is interesting to consider the findings of Zehe et al. (2021) that showed a clear correlation between the field's heterogeneity measure (statistical variance of the field's conductivity) and the self-organization of the field's transport, as represented by the Shannon entropy of the solute concentration matrix, in non-reactive transport in heterogeneous fields. Their results showed a clear decrease in Shannon entropy following an increase in the field's heterogeneity. These results are given further confirmation in our study, as, with the passage of time, the development of the reactive process in an initially
720 homogeneous field results in an increase of its heterogeneity (Figure 2b), accompanied by a decrease in the Shannon entropy of the transport in the field that corresponds to an increase in transport self-organization (Figure 3). To conclude our findings thus far, we state that the reactive transport at lower Peclet numbers, corresponding to diffusion-dominated flow, results in a higher field heterogeneity and, thus, stronger transport self-organization in the field. An important note should be made regarding the initial state of the field that undergoes reactive process: in our case of an initially homogeneous field, diffusion acts as
725 self-organization enhancer; in an initially heterogeneous case, diffusion is capable of decreasing the transport self-organization due to its smoothing property.

The Peclet number scalability is also exhibited in the Shannon entropy of transport self-organization. Assuming again separation of variables in $\tilde{S}_{norm}$, so that $\tilde{S}_{norm} = f(\tilde{t}) \cdot g(Pe)$ and the Peclet dependency takes on the form $g(Pe) = a \cdot 2^{-\cdot Pe} + b$,
730 satisfying results were obtained for $a, b = -0.02665, -0.000273$ ($R^2 = 0.9942$). Thus, the mean normalized Shannon entropy of transport self-organization depends on the reciprocal of 2 to the power of Peclet number.The free coefficient c is expected to be zero, since in the high-Peclet limit we expect to obtain no transport self-organization in the field; deviation from this value is attributed to statistical errors that can be decreased by averaging results from several realizations of the reactive process. The scaled curves are depicted in the figure inset. This dependence of the mean normalized Shannon entropy of transport
735 self-organization on the Peclet number confirms that this dimensionless number is indeed the driving force behind the transport self-organization in an initially homogeneous porous medium. The presented Peclet-dependency trends are reminiscent of the parameters that characterize the evolution of the reactive process in the field, analyzed in Section 4.1. They can be justified by directly relating the transport self-organization in the field to heterogeneity, which in turn is related to the global reaction rate in the field, for which the Peclet dependence was shown in an analytical result, derived in Section 3.1 (see also discussion in
740 Section 4.1).

Here, again, the relatively small scale of the presented phenomenon must be pointed out, although the apparent tendencies are clear. Had the model been allowed to run longer, further increase in heterogeneity would lead to a more pronounced decrease in the Shannon entropy of the transport. The dependency on the reciprocal of Peclet is expected to persist as long as
745 the degree of heterogeneity of the field remains moderate (see Section 3.1). The incompleteness of the Shannon entropy as a measure of transport self-organization in the field should be pointed out, since it does not take into account spatial correlations
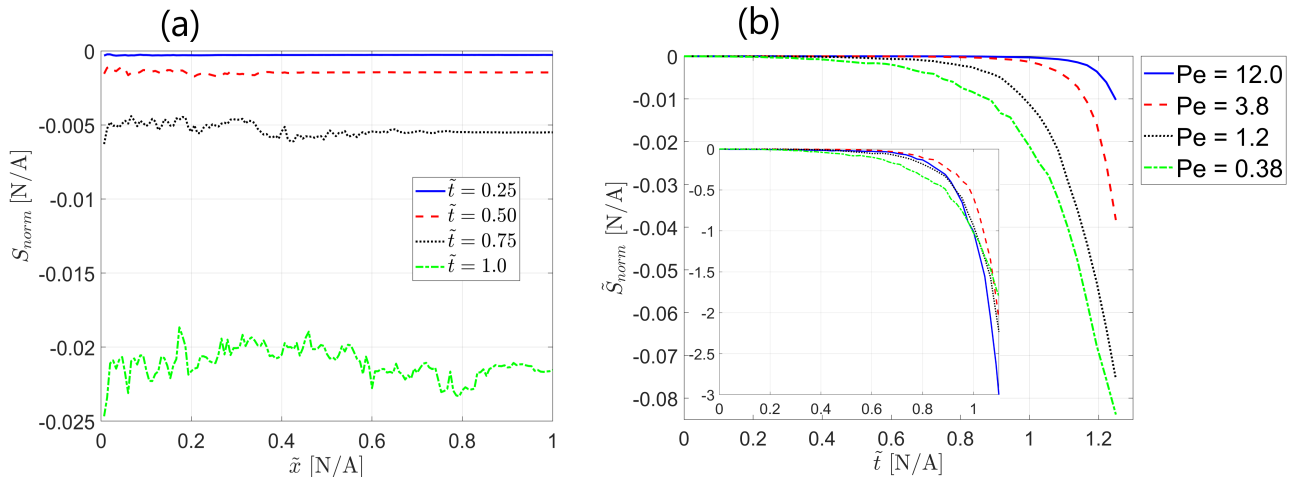
Figure 4. Self-organization of the transport in the field via normalized Shannon entropy $S_{norm} = (S - S_{max})/S_{max}$: (a) S_{norm} vs. normalized distance from inlet $\tilde{x} = x/L$ at different dimensionless times $\tilde{t}$ for $Pe = 0.38$, (b) Mean value of the normalized entropy over the field $\tilde{S}_{norm}$ vs. dimensionless time $\tilde{t}$ for different values of Pe. Inset shows Peclet-scaled curves, obtained by assuming a power-law Peclet dependency.

that may be present in the transport configuration in the field. However, it might be accurate enough for the specific case of an initially homogeneous field, as presented in the manuscript, since in this case the self-organization mimics the form of straight parallel channels from inlet to outlet. Thus, spatial correlation will not bear any additional information in this case, as 750 no larger-scale structures are expected to emerge in the field.

4.3 Entropy export into the break through curve

As a next stage in the analysis of transport self-organization in the reactive field, we turn to the particle breakthrough curve in an attempt to analyze the influence of self-organization of the field's transport on the particle arrival times. Figure 5a shows the temporal breakthrough curves calculated from the non-reactive particle tracking tests performed on the snapshots of the 755 reacting field for $Pe = 0.38$, as described in Section 3.2. The arrival times T_{BT} are normalized by the pore volume time T_{pv}. The width of support of the breakthrough curves clearly increases with time, indicating an increasing scatter in non-reactive particles arrival times as the field's heterogeneity grows larger. Especially, a significant increase in the tailing arrival times is observed.

760 The Shannon entropy of the breakthrough curves was calculated by dividing the arrival times span into 1000 bins and employing equation (19) with p_i as the relative occurrences of arrival times. To place all results on equal footing, the arrival time span was taken identical for all Peclet values. Figure 5b presents the normalized breakthrough curve entropy, calculated as $S_{norm}^{BTC} = (S^{BTC} - S_{max})/S_{max}$, vs. dimensionless time $\tilde{t}$. Here, S^{BTC} is the breakthrough curve entropy, calculated from
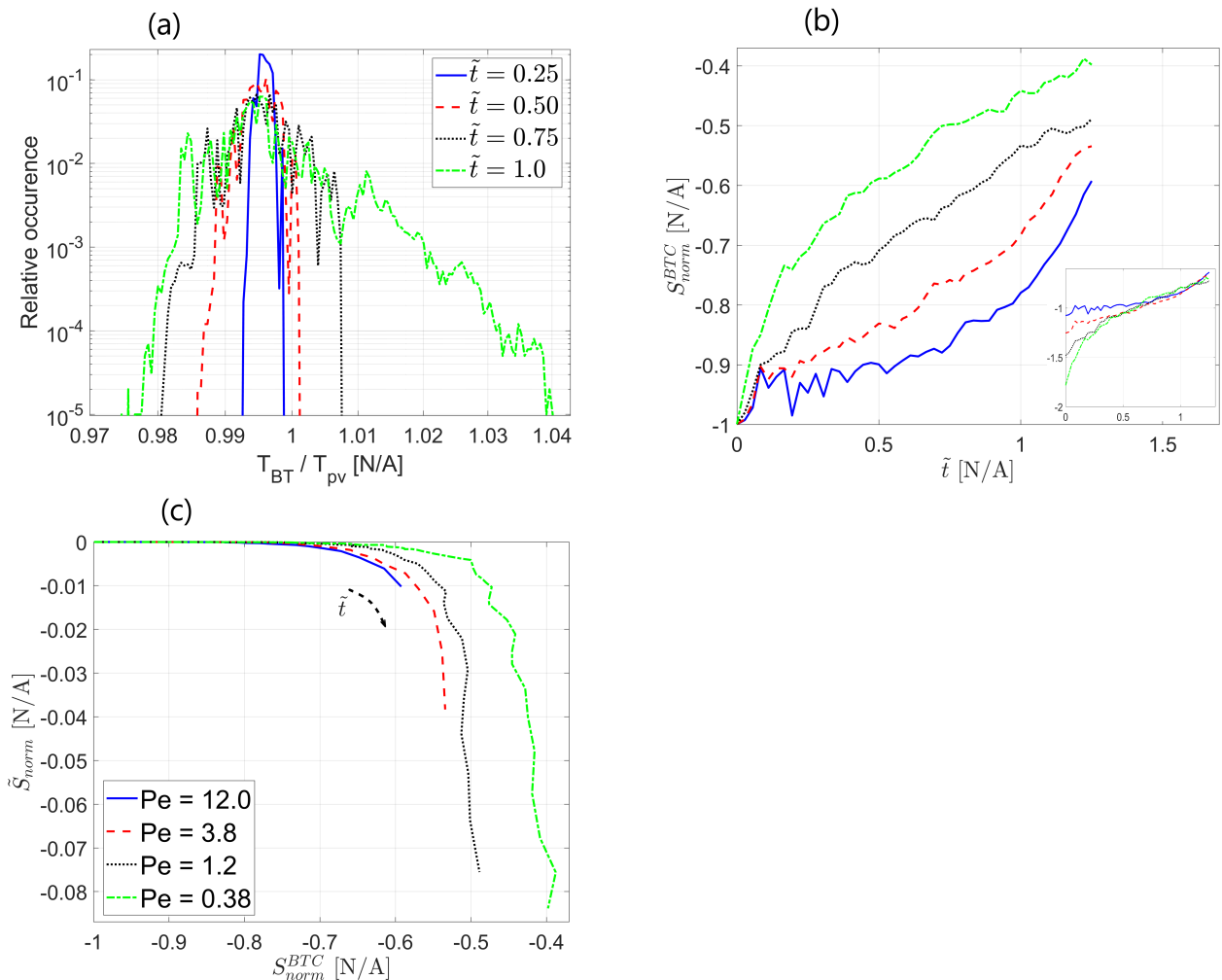
Figure 5. Breakthrough curve self-organization: (a) Histogram of the non-reactive particle arrival times T_{BT}, normalized by the pore volume time T_{pv}, in snapshots of the reacting field at different dimensionless times $\tilde{t}$ for $Pe = 0.38$, (b) Normalized breakthrough curve entropy S_{norm}^{BTC} vs. dimensionless time $\tilde{t}$ for different values of Peclet number (the inset shows Peclet-scaled curves) and (c) Normalized field transport entropy $\tilde{S}_{norm}$ vs. Normalized breakthrough curve entropy S_{norm}^{BTC} for different values of Peclet number. Time direction is specified by an arrow.

(19) and S_{max} is the maximal possible entropy value, obtained in the case of a perfectly uniform distribution of arrival times (similarly to the discussion of S_{max} estimation for the field transport entropy held in Section 3.2, in the case of division of the arrival times span into 1000 bins, this value will be $\log_2 1000$). Again, S_{norm}^{BTC} obtains values from 0 (no self-organization) to -1 (maximum self-organization, corresponding to the case when all particles arrive at the outlet at the same time). A picture emerges, where the Shannon entropy of the arrival times increases with the passage of time, reflecting a larger uncertainty and a

declining order in the temporal distribution of travel times. This corresponds to an increase in both the field's heterogeneity and
the self-organization of transport, as the reactive process in the field evolves. We also observe that the level of self-organization
in arrival times directly correlates with the Peclet number, as the normalized breakthrough entropy S_{norm}^{BTC} decreases with increase in Peclet, an opposite tendency comparing to the entropy of the field transport (see Section 4.2).

The Peclet number scalability is also exhibited in the Shannon entropy of the breakthrough curve, from approximately $\tilde{t} = 0.5$. Assuming again separation of variables in S_{norm}^{BTC}, so that $S_{norm}^{BTC} = f(\tilde{t}) \cdot g(Pe)$ and the Peclet dependency takes on the power law form $g(Pe) = a \cdot Pe^b + c$, satisfying results were obtained for $a, b, c = 0.5511, -0.1686, -1.0$ ($R^2 = 0.9762$). The free coefficient c obtains the value of -1, because in the high-Peclet limit we expect to obtain maximal self-organization in the breakthrough times. The trends presented in Figure 5b are further supported by Figure 5c that shows the normalized field transport entropy $\tilde{S}_{norm}$ as a function of the normalized breakthrough curve entropy S_{norm}^{BTC} for different values of Peclet number: $\tilde{S}_{norm}$ decreases monotonously with an increase in S_{norm}^{BTC} for all values of Peclet number. These results can be explained straight-ahead in terms of the degree of the field's heterogeneity: for lower Peclet values, the reactive transport in the field leads to a higher degree of heterogeneity, which is responsible for a greater scattering in arrival times due to the variety of paths particles may take on their way to outlet; this is reflected in the overall smoothing out of the breakthrough curve and, as a result, in the breakthrough curve entropy that grows with the degree of scattering in arrival times. ~~An alternative observing perspective on the arrival times can be formulated in thermodynamic terms Zehe et al. (2021): since the transport entropy within the field is decreasing for lower Peclet values and~~ While there are other factors that affect the total entropy budget of the problem, such as production of the macroscopic flow entropy due to hydraulic power dissipation through heat, these two properties are correlated in a self-consistent way. Thus, a thermodynamic analogy can be made: since, according to the second law of Thermodynamics, the overall entropy of the system and its surroundings cannot decrease, the ~~entropy~~ decreasing entropy of the system, represented, among other contributions, by the entropy of the transport in the field, ~~produced within the field~~ needs to be exported outside~~, leading~~. This leads to an increase in the entropy of ~~its surroundings~~ the surroundings, which is reflected, among other factors, in an increase of the temporal breakthrough curve entropy (see Appendix A in the Supplementary data)~~; this is reflected in the increased entropy of the breakthrough curve. This statement~~. This analogy should be regarded on a qualitative level only~~, as, due to different spatial and temporal discretizations, changes in the Shannon entropies of the field transport and the breakthrough curves with the passage of time do not comply.~~.

4.4 Hydraulic power - entropy relation

The evolution of the reactive process in an initially homogeneous field is accompanied by the emergence of heterogeneity and, consequently, transport self-organization in the field. This demands that an increased energy is supplied to the field to maintain an increasingly ordered state that emerges there. This energy is supplied in the form of hydraulic power, required for the flow to overcome the hydraulic resistance of the porous medium. In our model, the hydraulic power is supplied due to the inlet-outlet hydraulic head drop boundary condition applied to the porous medium, that works similarly to a pump.
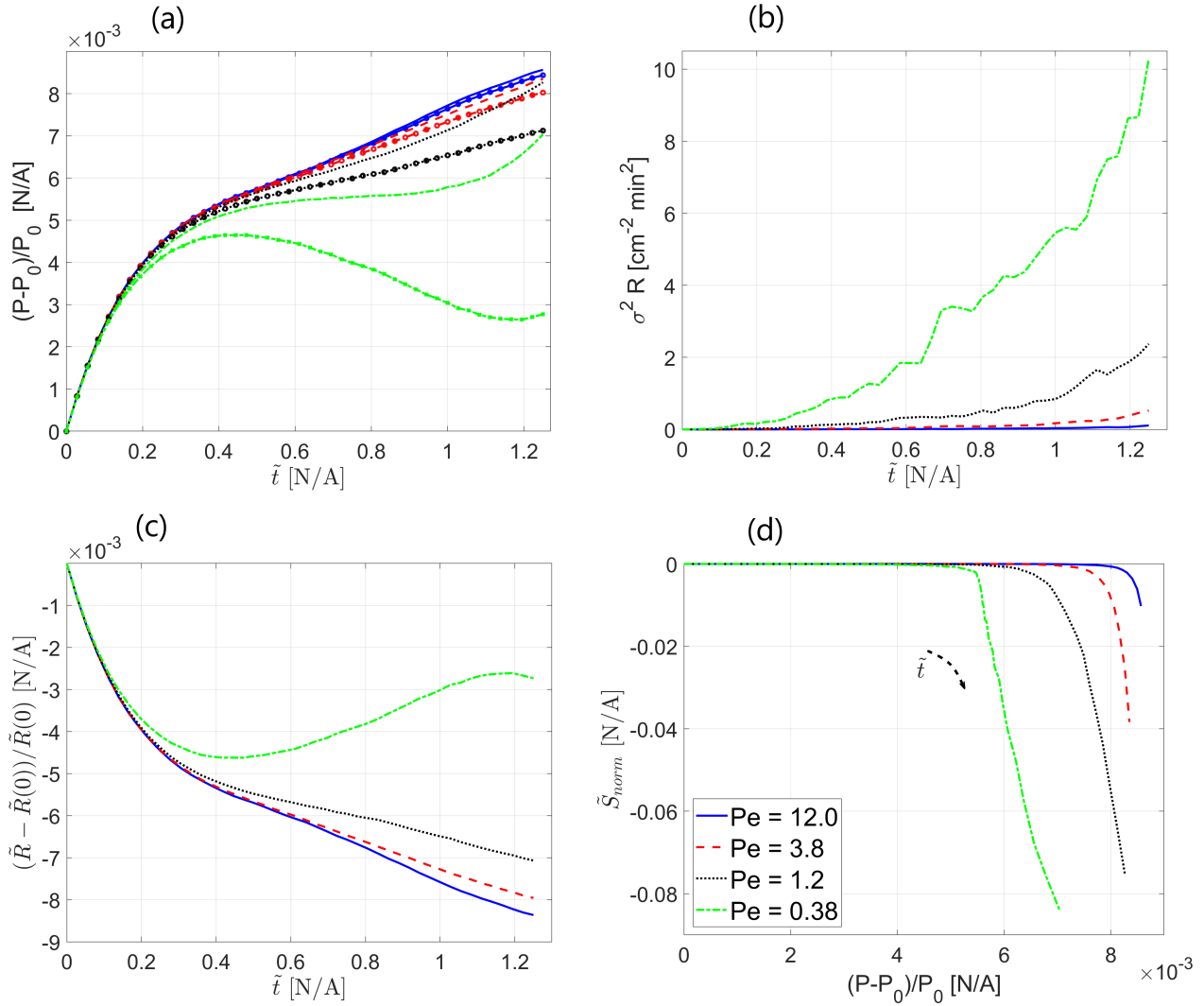
Figure 6. Hydraulic power in the field and its relation to heterogeneity and transport entropy: (a) Normalized hydraulic power vs. dimensionless time $\tilde{t}$ (solid lines represent cell-wise power calculation P_{total}, while the dashed lines represent power, calculated based on the parallel channels model P_{total}^{EQ}), (b) Variance of the channel hydraulic resistivities $\sigma^2 R$ vs. dimensionless time $\tilde{t}$, (c) Mean value of the channel hydraulic resistivities $\tilde{R}$, normalized by the value at $\tilde{t} = 0$ vs. dimensionless time $\tilde{t}$, and (d) Normalized mean field transport entropy $\tilde{S}_{norm}$ vs. Normalized hydraulic power $(P - P_0)/P_0$, for different values of Peclet number. Time direction is specified by an arrow.

Figure 6a presents the Normalized hydraulic power in the field $(P - P_0)/P_0$ as a function of dimensionless time $\tilde{t}$ for different Peclet numbers, calculated using different approaches (see Section 3.3). Here, the solid lines represent cell-wise power calculation (P_{total}, according to (20)), while the dashed lines represent power, calculated based on the parallel channels model (P_{total}^{EQ}, according to (23)). Due to the linearity of the observed preferential flow paths, as presented in Figure 3, the channels in the simplified model used to calculate P_{total}^{EQ} were assumed to be of a linear shape, thus the indices i, j in (22) correspond to the rows and columns of the computational field. In both approaches, the power is calculated over the whole field. From this comparative plot it is evident that, for all Peclet numbers, the power increases with $\tilde{t}$, along with the increase in heterogeneity of the field, and that is in accordance with our expectations as detailed in Section 3.3. We also observe that the parallel channel assumption is valid as a rule in the initial part of the reactive process, however, as the normalized time $\tilde{t}$ grows, the deviations from this assumption increase. This can be explained by the fact that P_{total}^{EQ}, calculated under this assumption, takes into account only the power produced by the horizontal Darcy flux component, since the parallel channel model does not allow interaction between adjacent channels, while P_{total}, calculated in a cell-wise fashion, accounts also for the transverse (vertical) flux component. With the passage of time, due to an increase in heterogeneity of an initially homogeneous field, flux in the transverse direction appears. With time, its contribution grows as it appears more significant. We observe that until about $\tilde{t} = 0.4$, the parallel channel assumption appears adequate for all Peclet values. Beginning from $\tilde{t} = 0.4$, deviations from this assumption are visible. The magnitude of these deviations is in direct correlation with the Peclet number and increases with the decrease in Peclet. This can be explained again by virtue of heterogeneity, which increases with the decrease in Peclet, as well as with $\tilde{t}$.

The confirmation to the proposition put forth in Section 3.3, that relates the increase in the total hydraulic power dissipated in the field to an increase in heterogeneity of field by virtue of the simplified parallel channels model, is given in Figure 6b that presents the Variance of the hydraulic resistivities of the channels $\sigma^2 R$ vs. dimensionless time $\tilde{t}$. We observe that $\sigma^2 R$ increases monotonously with $\tilde{t}$, as the overall field heterogeneity grows larger, signifying the underlying relation between heterogeneity and the dissipated power in the field. It is also interesting to notice that, although the increase in the heterogeneity of the field is largest for the lower values of the Peclet number, the Normalized hydraulic power, presented in Figure 6a, grows faster for higher Peclet values. The explanation for this lies in the fact that, along with increasing the heterogeneity of the field, the coupled reactive dissolution / precipitation process also works to increase the mean value of the hydraulic conductivity in the field (see Section 4.1). This also contributes to an increase in the total hydraulic power in the field, as can be seen from (24). ~~A~~ The confirmation for this can be seen in Figure 6c, that presents the Mean value of the channel hydraulic resistivities $\tilde{R}$, normalized by the value at $\tilde{t} = 0$, vs. dimensionless time $\tilde{t}$. We observe that $\tilde{R}$ decreases with time, meaning that ~~their~~ the channels' mean conductivity grows larger; this is in accordance with Figure 2c. However, we also observe that faster decrease rates are observed for the higher Peclet values, which contradicts the trends presented in Figure 2c. This apparent contradiction is due to the fact that in the hydraulic power calculation the entire field was taken into account, as opposed to parameters presented in Figure 2, where an area of 10 computational cell columns in the immediate vicinity of the outlet was left out to exclude the effect of the dissolution area there. Thus, when including the dissolution area at the inlet into calculation, we

observe the Peclet-dependency trends overturn; at the inlet, more dissolution occurs for the higher Peclet values due to a clear bias towards dissolution, since no B particles are present there. Thus, the behavior of the Normalized hydraulic power in the field (Figure 6a) is controlled by the combined effect of two parameters: the variance of the channel hydraulic resistivities $\sigma^2 R$ (Figure 6b) and the mean value of the channel hydraulic resistivities $\tilde{R}$ (Figure 6c).

Finally, Figure 6d presents the Normalized mean field transport entropy $\tilde{S}_{norm}$ as a function of the net hydraulic power $(P - P_0)/P_0$ for different values of the Peclet number. This plot shows the expected relation between the entropy of the transport and the Normalized hydraulic power in the field: for each Peclet number, the entropy of the transport in the field decreases with an increase in the Normalized hydraulic power, reflecting an increase in transport self-organization due to an increase in power, supplied to the field in order to maintain the prescribed hydraulic pressure drop boundary condition over the field.

5 Conclusions

Our computational study tackles the quantitative characterization of the transport self-organization that emerges in an initially homogeneous calcite porous medium due to the dynamic interaction between the reactive precipitation / dissolution processes and the solute transport. Our work leads to the following key conclusions:

- As the reactive particles advance and react in an initially homogeneous field, heterogeneity is being introduced into the field in the form of local dissolution / precipitation areas, evolving further downstream and intensifying with time. A dissolution area is located in the immediate vicinity of the inlet, where the chemical equilibrium is tilted towards dissolution; this correlates with experimental and simulation observations. The global reaction rate, normalized by the distance from inlet sampled by the flow, is shown to be approximately constant in time. The influence of the Peclet number is exhibited by an increase in the global reaction rate with the decrease in Peclet, thus confirming that the diffusive transport mechanism, responsible for the mixing in the field, enhances reactive process. This can be explained by the fact that diffusion, being stochastic in nature, allows particles to sample regions away from the path suggested by the advection mechanism, thus allowing a better chance for reaction. The net reaction is tilted towards dissolution, as the mean conductivity value in the field grows monotonously with time, as well as with the Peclet number, which is reasonable due to the influx of low pH fluid at the inlet of the field. Similar trends are observed in the evolution of the variance of hydraulic conductivity in the field. Scalability of the parameters that characterize the evolution of the reactive process in the field with the reciprocal of the Peclet number was derived using a simple one-dimensional ADRE model with linear adsorption reaction term and then confirmed through numerical simulations, with the global reaction rate, the mean value and the variance of the hydraulic conductivity distribution in the field all exhibiting dependency on the reciprocal of the Peclet number. We thus state that reactive transport scenarios for lower Peclet values, corresponding to dominant diffusive transport mechanism, coincide with an increased global reaction rate in the field and, thus, an increase in the field's heterogeneity. The dependence of the parameters that characterize the reactive process in the field

870   on the reciprocal of the Peclet number confirms that this dimensionless number is indeed the driving force behind the evolution of the reactive process in the porous medium.

- As the reactive processes in the field advance, the evolving variations in the hydraulic conductivity of the field create an autocatalytic feedback mechanism that leads to an emergence of finger-like preferential flow paths of a linear shape. These paths interact, competing for the available flow, so that eventually some of the paths carry a significantly larger part

875   of the injected particles than the others, as seen from the increasing concentration gradients in the direction transverse to flow. This observation is confirmed by the mean normalized Shannon entropy in the field that decreases with time, signifying an increase in the level of transport self-organization in the field. The influence of the Peclet number on the evolution of transport self-organization is exhibited by a decrease in the mean normalized Shannon entropy of the transport with a decrease in Peclet, signifying an increase in self-organization. This clearly indicates that diffusion is

880   the dominant mechanism in creating self-organization in the initially homogeneous field. Here the link between the emergence of heterogeneity and transport self-organization in an initially homogeneous field is being drawn, as the increase in heterogeneity results in the increase in the level of self-organization of the transport in the field. Peclet number scalability was shown for the mean normalized Shannon entropy curves as well. To conclude, we state that reactive transport at lower Peclet numbers, corresponding to diffusion-dominated flow, results in a higher field heterogeneity and,

885   thus, stronger transport self-organization in the field. An important note should be made regarding the initial state of the field that undergoes the reactive process: in the case of an initially homogeneous field, diffusion acts as self-organization enhancer; in an initially heterogeneous case, diffusion is capable of decreasing the transport self-organization due to its smoothing property.

- To switch the observing perspective, the particle temporal breakthrough curve was analyzed in an attempt to understand

890   the influence of self-organization of the field's transport on the particle arrival times. The width of support of the break-through curve clearly increases with time, as the reactive process in the field evolves, indicating an increasing scatter in arrival times of non-reactive particles; this result is in line with an increase in the field's heterogeneity. A picture emerges, where the Shannon entropy of the arrival times increases with the passage of time, reflecting a larger uncertainty and a declining order in the temporal distribution of travel times. We also observe that the level of self-organization

895   in arrival times directly correlates with the Peclet number, as the normalized breakthrough curve entropy decreases with increase in Peclet, an opposite tendency comparing to the entropy of the field transport. ~~An explanation to this can be formulated in thermodynamic terms:~~ While there are other factors that affect the total entropy budget of the problem, such as production of the macroscopic flow entropy due to hydraulic power dissipation through heat, these two properties are correlated in a self-consistent way. Thus, a thermodynamic analogy can be made: since, according to the second law

900   of Thermodynamics, the overall entropy of the system and its surroundings cannot decrease, ~~therefore the decreasing transport entropy~~ the decreasing entropy of the system, represented, among other contributions, by the entropy of the transport in the field, needs to be exported outside~~, leading~~. This leads to an increase in the entropy of the surroundings~~;~~

~~this is reflected~~, which is reflected, among other factors, in an increase of the temporal breakthrough curve entropy. This analogy should be regarded on a qualitative level only.

905   – The evolution of the reactive process in an initially homogeneous field, accompanied by the emergence of heterogeneity and, consequently, transport self-organization in the field, demands that an increased energy is supplied to the field to maintain an increasingly ordered state that emerges therein. This energy is supplied in the form of hydraulic power, required for the flow to overcome the hydraulic resistance of the porous medium. We observe that, for all Peclet numbers,

910 the total dissipated hydraulic power increases with time, along with the increase in heterogeneity and mean hydraulic conductivity of the field, confirming the trends suggested by a simple parallel channels model. The entropy of the transport in the field decreases with an increase in the hydraulic power, reflecting an increase in transport self-organization. This increasing power is supplied to the field in order to maintain the hydraulic head drop boundary condition due to an increase in the field's heterogeneity. Following our thermodynamic framework, we thus argue that the power, required to maintain the driving head pressure drop boundary condition between inlet and outlet, increases with the increasing

915 variance of the hydraulic conductivity in the field due to the evolution of the reactive process therein (although the contribution of an increase in the mean conductivity value also shouldn't be forgotten in this context). This increase in the supplied power results in an increase in the level of transport self-organization in the field.

  – To conclude, the scenario presented in the manuscript corresponds to that of an open thermodynamic system that interacts with its surroundings by exchanging matter and energy. Due to influx of power from outside, this system is kept in a

920 non-equilibrium state that corresponds to a certain degree of internal self-organization and, thus, to a decreased entropy state. ~~Since, according to the 2nd law of Thermodynamics, the overall entropy of the system and its surroundings cannot decrease , this decrease~~ This decrease in entropy of a system corresponds to an increase in entropy of the surroundings by means of ~~exporting entropy from the system outside. Thus, such a system exhibits a pattern, characterized by~~ production of entropy in the system through various processes, which is later being exported outside. In our system, we

925 investigate the interplay between ~~the three thermodynamic properties: entropy of~~ three thermodynamic parameters: the entropy of transport self-organization within the field, the ~~system,~~ entropy of the ~~surroundings and~~ breakthrough curve and the hydraulic power, dissipated by the flow, which may be viewed as an influx of power required to maintain the current level of the system's self-organization. ~~In our system, these three properties are represented by the entropy of transport self-organization within the field, the entropy of the breakthrough curve and the hydraulic power , dissipated~~

930 ~~by the flow as it passes within the field.~~ While there are additional processes that may influence the overall entropy budget, such as production of the macroscopic flow entropy due to hydraulic power dissipation through heat, we find that these three properties are correlated in a self-consistent way. The contribution of the above-mentioned additional factors are beyond the scope of the current study. The increase in the hydraulic power, dissipated in the field, as well as the emergence of transport self-organization, are both the result of an increase in the heterogeneity of the field (although

935 the contribution of an increase in the value of the mean hydraulic conductivity to the hydraulic power also shouldn't be overlooked). The latter, in turn, can be viewed as a consequence of the energy invested in the field by the dissolution /

precipitation reactive process. We emphasize that the presented study does not intend to construct a complete thermo-dynamic formalism for the problem under investigation. The thermodynamic framework presented in the current study is aimed at providing qualitative dependencies / trends between the above-mentioned parameters of interest, such as the entropy of the transport self-organization, the hydraulic power, dissipated in the field, etc. It is our intent to arrive at a more complete thermodynamic formalism for the reactive flow in porous medium in the course of the research work.

- Employing thermodynamic framework to investigate the dynamic reaction-transport interaction in porous media may prove beneficial whenever the need exists to establish relations between the intensification of the preferential flow path phenomenon, represented by the decline in Shannon entropy of the transport, to the amount of reaction that occurred in the porous medium and the change in its heterogeneity. This can be of considerable significance to implications of reactive-transport interaction in various geophysical applications and assist, for example, in estimation of efficient ways to remediate soil contamination, determination of optimal conditions for CO_2 sequestration and estimation of oil extraction rates from the borehole.

Code and data availability. A dedicated repository, containing all codes and data, will be created on GitHub.

Author contributions. ES developed the research methodology, wrote major parts of the simulation code, performed numerical simulations, analyzed data, and wrote the manuscript. YE supervised the implementation of the research methodology, supplied the initial version of the simulation code, and oversaw the writing of the manuscript.

Competing interests. The authors have no competing interests to declare.

Acknowledgements. Y.E. and E.S. thank the support of the Israel Science Foundation (grant No.801/20).

955 References

Ajayi, T., Gomes, J. S., and Bera, A.: A review of CO2 storage in geological formations emphasizing modeling, monitoring and capacity estimation approaches, Water Resources research, 50, 1490–1505, https://doi.org/https://doi.org/10.1002/2013WR015111, 2014.

Al-Khulaifi, Y., Lin, Q., Blunt, M. J., and Bijeljic, B.: Reaction Rates in Chemically Heterogeneous Rock: Coupled Impact of Structure and Flow Properties Studied by X-ray Microtomography, Environmental Science Technology, 51(7), 4108–4116,
960 https://doi.org/https://doi.org/10.1021/acs.est.6b06224, 2017.

Bear, J. and Cheng, A.: Modeling Groundwater Flow and Contaminant Transport, vol. 23, https://doi.org/10.1007/978-1-4020-6682-5, 2010.

Ben-Naim, A.: A Farewell to Entropy, WORLD SCIENTIFIC, https://doi.org/10.1142/6469, 2008.

Berkowitz, B. and Zehe, E.: Surface water and groundwater: unifying conceptualization and quantification of the two "water worlds", Hydrology and Earth System Sciences, 24, 1831–1858, https://doi.org/https://doi.org/10.5194/hess-24-1831-2020, 2020.

965 Berkowitz, B., Dror, I., and Yaron, B.: Contaminant Geochemistry. Interactions and Transport in the Subsurface Environment, Springer-Verlag, Berlin, 2014.

Berkowitz, Y., Edery, Y., Scher, H., and Berkowitz, B.: Fickian and non-Fickian diffusion with bimolecular reactions, Phys. Rev. E, 87, 032 812, https://doi.org/10.1103/PhysRevE.87.032812, 2013.

Beven, K. and Germann, P.: Macropores and Water Flow in Soils, Water Resources Research - WATER RESOUR RES, 18, 1311–1325,
970 https://doi.org/10.1029/WR018i005p01311, 1982.

Borgne, T. L., Dentz, M., and Ramírez, J. C.: Lagrangian Statistical Model for Transport in Highly Heterogeneous Velocity Fields, Physical Review Letters, 101, 090 601, https://doi.org/DOI:10.1103/PhysRevLett.101.090601, 2008.

Brusseau, M. L.: Transport of reactive contaminants in heterogeneous porous media, Reviews of Geophysics, 32, 285–313, https://doi.org/https://doi.org/10.1029/94RG00624, 1994.

975 Camazine, S., Deneubourg, J.-L., Franks, N. R., Sneyd, J., Theraula, G., and Bonabeau, E.: Self-Organization in Biological Systems, Princeton University Press, 2001.

Chiogna, G. and Rolle, M.: Entropy-based critical reaction time for mixing-controlled reactive transport, Water Resources Research, 53, 7488–7498, https://doi.org/https://doi.org/10.1002/2017WR020522, 2017.

Clausius, R.: Uber die Art der Bewegung, welche wir Warme nennen, Annalen der Physik und Chemie, 79, 353–380, 1857.

980 Deng, H., Poonoosamy, J., and Molins, S.: A reactive transport modeling perspective on the dynamics of interface-coupled dissolution-precipitation, Applied Geochemistry, 137, 105 207, https://doi.org/https://doi.org/10.1016/j.apgeochem.2022.105207, 2022.

Domenico, P. A. and Schwartz, F. W.: Physical and Chemical Hydrogeology, 2nd Edition, John Wiley & sons Ltd., 1997.

Edery, Y., Scher, H., and Berkowitz, B.: Modeling bimolecular reactions and transport in porous media, Geophysical Research Letters, 36, https://doi.org/https://doi.org/10.1029/2008GL036381, 2009.

985 Edery, Y., Scher, H., and Berkowitz, B.: Particle tracking model of bimolecular reactive transport in porous media, Water Resources Research, 46, https://doi.org/https://doi.org/10.1029/2009WR009017, 2010.

Edery, Y., Scher, H., and Berkowitz, B.: Dissolution and precipitation dynamics during dedolomitization, Water Resources Research, 47, https://doi.org/https://doi.org/10.1029/2011WR010551, 2011.

Edery, Y., Guadagnini, A., Scher, H., and Berkowitz, B.: Reactive transport in disordered media: Role of fluctuations in interpretation of
990 laboratory experiments, Advances in Water Resources, 51, 86–103, https://doi.org/https://doi.org/10.1016/j.advwatres.2011.12.008, 35th Year Anniversary Issue, 2013.

Edery, Y., Guadagnini, A., Scher, H., and Berkowitz, B.: Origins of anomalous transport in heterogeneous media:Structural and dynamic controls, Physical Review, 99, https://doi.org/https://doi.org/10.1103/PhysRevE.99.033108, 2014.

Edery, Y., Geiger, S., and Berkowitz, B.: Structural controls on anomalous transport in fractured porous rock, Water Resources Research, 52, 5634–5643, https://doi.org/https://doi.org/10.1002/2016WR018942, 2016a.

Edery, Y., Porta, G., Guadagnini, A., Scher, H., and Berkowitz, B.: Characterization of Bimolecular Reactive Transport in Heterogeneous Porous Media, Transport in Porous Media, 115, 291–310, https://doi.org/https://doi.org/10.1007/s11242-016-0684-0, 2016b.

Edery, Y., Stolar, M., Porta, G., and Guadagnini, A.: Feedback mechanisms between precipitation and dissolution reactions across randomly heterogeneous conductivity fields, Hydrol. Earth Syst. Sci., pp. 5905—5915, https://doi.org/https://doi.org/10.5194/hess-25-5905-2021, 2021.

Guadagnini, A. and Neuman, S. P.: Nonlocal and localized analyses of conditional mean steady state flow in bounded, randomly nonuniform domains: 1. Theory and computational approach, Water Resources Research, 35, 2999–3018, https://doi.org/https://doi.org/10.1029/1999WR900160, 1999.

Haken, H.: Synergetics : an introduction: nonequilibrium phase transitions and self-organization in physics, chemistry, Springer series in synergetics, v.1, Springer-Verlag Berlin Heidelberg, 1983.

Hansen, A., Sinha, S., Bedeaux, D., Kjelstrup, S., Gjennestad, M. A., and Vassvik, M.: Relations Between Seepage Velocities in Immiscible, Incompressible Two-Phase Flow in Porous Media, Transport in Porous Media, 125, 565–587, https://doi.org/https://doi.org/10.1007/s11242-018-1139-6, 2018.

Hansen, A., Flekkøy, E. G., Sinha, S., and Slotte, P. A.: A statistical mechanics framework for immiscible and incompressible two-phase flow in porous media, Advances in Water Resources, 171, 104 336, https://doi.org/https://doi.org/10.1016/j.advwatres.2022.104336, 2023.

Hemelrijk, C. K. and Hildenbrandt, H.: Schools of fish and flocks of birds: their shape and internal structure by self-organization, Interface Focus, 2, https://doi.org/https://doi.org/10.1098/rsfs.2012.0025, 2012.

Jiao, T., Ye, M., Jin, M., and Yang, J.: A finite particle method (FPM) for Lagrangian simulation of conservative solute transport in heterogeneous porous media, Advances in Water Resources, 156, 104 043, https://doi.org/https://doi.org/10.1016/j.advwatres.2021.104043, 2021.

Kamolpornwijita, W., Liangb, L., Westa, O., Molinea, G., and Sullivan, A.: Preferential flow path development and its influence on long-term PRB performance: column study, Journal of Contaminant Hydrology, 66, 161–178, https://doi.org/https://doi.org/10.1016/S0169-7722(03)00031-7, 2003.

Kloeden, P. E.: Numerical solution of stochastic differential equations, Applications of mathematics; v. 23, Springer, Berlin, 1992.

Kondepudi, D. and Prigogine, I.: Modern Thermodynamics: From Heat Engines to Dissipative Structures, John Wiley & sons Ltd., 1998.

Kreft, A. and Zuber, A.: On the physical meaning of the dispersion equation and its solutions for different initial and boundary conditions, Chemical Engineering Science, 33, 1471–1480, https://doi.org/https://doi.org/10.1016/0009-2509(78)85196-3, 1978.

Ladd, A. and Szymczak, P.: Reactive Flows in Porous Media: Challenges in Theoretical and Numerical Methods, Annual Review of Chemical and Biomolecular Engineering, 12, 543–571, https://doi.org/10.1146/annurev-chembioeng-092920-102703, 2021.

Leone, F. C., Nelson, L. S., and Nottingham, R. B.: The Folded Normal Distribution, Technometrics, 3, 543–550, https://doi.org/10.1080/00401706.1961.10489974, 1961.

Li, W., Einstein, H. H., and Germaine, J. T.: An Experimental Study of Matrix Dissolution and Wormhole Formation Using Gypsum Core Flood Tests: 1. Permeability Evolution and Wormhole Geometry Analysis, Journal of Geophysical Research: Solid Earth, 124, https://doi.org/https://doi.org/10.1029/2018JB017238, 2019.

1030 Manahan, S.: Environmental Chemistry, 9th ed., CRC Press, 2000.

Mays, D. C., Faybishenko, B. A., and Finsterle, S.: Information entropy to measure temporal and spatial complexity of unsaturated flow in heterogeneous media, Water Resources Research, 38, https://doi.org/https://doi.org/10.1029/2001WR001185, 2002.

Meakin, P. and Tartakovsky, A. M.: Modeling and simulation of pore-scale multiphase fluid flow and reactive transport in fractured and porous media, Reviews of Geophysics, 47, https://doi.org/https://doi.org/10.1029/2008RG000263, 2009.

1035 Morse, J. and Mackenzie, F.: Geochemistry of Sedimentary Carbonates, Vol. 48, 1st Edition, Developments in Sedimentology, Elsevier Science, 1990.

Nguyen, V. and Papavassiliou, D. V.: Hydrodynamic Dispersion in Porous Media and the Significance of Lagrangian Time and Space Scales, Geochimica et Cosmochimica Acta, 5, https://doi.org/https://doi.org/10.3390/fluids5020079, 2020.

Nissan, A. and Berkowitz, B.: Reactive Transport in Heterogeneous Porous Media Under Different Péclet Numbers, Water Resources Re-
1040 search, 55, https://doi.org/https://doi.org/10.1029/2019WR025585, 2019.

Perez, L. J., Hidalgo, J. J., and Dentz, M.: Reactive Random Walk Particle Tracking and Its Equivalence With the Advection-Diffusion-Reaction Equation, Water Resources Research, 55, 847–855, https://doi.org/https://doi.org/10.1029/2018WR023560, 2019.

Petrosino, F., Rosa, D. D., and Mingione, G.: Application of different Lagrangian Particle Tracking techniques for water impingement, IOP Conference Series: Materials Science and Engineering, 1024, 012 011, https://doi.org/10.1088/1757-899X/1024/1/012011, 2021.

1045 Poonoosamy, J., Klinkenberg, M., Deissmann, G., Brandt, F., Bosbach, D., Mäder, U., and Kosakowski, G.: Effects of solution supersaturation on barite precipitation in porous media and consequences on permeability: Experiments and modelling, Geochimica et Cosmochimica Acta, 270, 43–60, https://doi.org/https://doi.org/10.1016/j.gca.2019.11.018, 2020.

Radolinski, J., Le, H., Hilaire, S. S., Xia, K., Scott, D., and Stewart, R. D.: A spectrum of preferential flow alters solute mobility in soils, Scientific Reports, 12, https://doi.org/https://doi.org/10.1038/s41598-022-08241-w, 2022.

1050 Raveh-Rubin, S., Edery, Y., Dror, I., and Berkowitz, B.: Nickel migration and retention dynamics in natural soil columns, Water Resources Research, 51, 7702–7722, https://doi.org/https://doi.org/10.1002/2015WR016913, 2015.

Risken, H.: The Fokker-Planck Equation: Methods of Solution and Applications, Springer Series in Synergetics, Springer Berlin Heidelberg, 1996.

Schmidt, M. J., Pankavich, S. D., Navarre-Sitchler, A., and Benson, D. A.: A Lagrangian method for reactive transport with solid/aqueous
1055 chemical phase interaction, Journal of Computational Physics: X, 2, 100 021, https://doi.org/https://doi.org/10.1016/j.jcpx.2019.100021, 2019.

Schrodinger, E.: What is Life?: With Mind and Matter and Autobiographical Sketches, Cambridge University Press, 1944.

Schweizer, D., Blum, P., and Butscher, C.: Uncertainty assessment in 3-D geological models of increasing complexity, Solid Earth, 8, 515–530, https://doi.org/https://doi.org/10.5194/se-8-515-2017, 2017.

1060 Shannon, C. E.: A Mathematical Theory Of Communication, Bell System Technical Journal, 782, 623–656, https://doi.org/https://doi.org/10.1002/j.1538-7305.1948.tb01338.x, 1948.

Shazly, A. E.: Acid Gas Injection into Petroleum Reservoirs: A Review, Petroleum and Petrochemical Engineering Journal, 5, https://doi.org/https://doi.org/10.23880/ppej-16000280, 2021.

Shirolkar, J., Coimbra, C., and Queiroz McQuay, M.: Fundamental aspects of modeling turbulent particle dispersion in dilute flows, Progress
1065 in Energy and Combustion Science, 22, 363–399, https://doi.org/https://doi.org/10.1016/S0360-1285(96)00006-8, 1996.

Singurindy, O. and Berkowitz, B.: Flow, Dissolution and Precipitation in Dolomite, Water Resources Research, 39, https://doi.org/https://doi.org/10.1029/2002WR001624, 2003.

Snippe, J., Berg, S., Ganga, K., Brussee, N., and Gdanski, R.: Experimental and numerical investigation of wormholing during CO2 storage and water alternating gas injection, International Journal of Greenhouse Gas Control, 94, https://doi.org/https://doi.org/10.1016/j.ijggc.2019.102901, 2020.

Sole-Mari, G. and Fernandez-Garcia, D.: Lagrangian Modeling of Reactive Transport in Heterogeneous Porous Media With an Automatic Locally Adaptive Particle Support Volume, Water Resources Research, 54, 8309–8331, https://doi.org/https://doi.org/10.1029/2018WR023033, 2018.

Sole-Mari, G., Fernàndez-Garcia, D., Sanchez-Vila, X., and Bolster, D.: Lagrangian Modeling of Mixing-Limited Reactive Transport in Porous Media: Multirate Interaction by Exchange With the Mean, Water Resources Research, 56, e2019WR026 993, https://doi.org/https://doi.org/10.1029/2019WR026993, 2020.

Stamm, C., Flühler, H., René, G., Leuenberger, J., and Wunderli, H.: Preferential Transport of Phosphorus in Drained Grassland Soils, Journal of Environmental Quality - J ENVIRON QUAL, 27, https://doi.org/10.2134/jeq1998.00472425002700030006x, 1998.

Stolum, H.: River Meandering as a Self-Organization Process, Science, 271, 1710–1713, https://doi.org/10.1126/science.271.5256.1710, 1996.

Szymczak, P. and Ladd, A.: A network model of channel competition in fracture dissolution, Geophysical Research Letters, 33, https://doi.org/https://doi.org/10.1029/2005GL025334, 2006.

Turing, A. M.: The Chemical Basis of Morphogenesis, Philosophical Transactions of the Royal Society of London. Series B, Biological Sciences, 237, 37–72, https://doi.org/https://doi.org/10.1098/rstb.1952.0012, 1952.

Woodbury, A. D. and Ulrych, T. J.: Minimum relative entropy inversion: Theory and application to recovering the release history of a groundwater contaminant, Water Resources Research, 32, 2671–2681, https://doi.org/https://doi.org/0043-1397/96/95WR-03818509.00, 1996.

Yan, X., Sun, Z., Li, S., Yang, W., and Zhang, Y.: Evaluation of Effectiveness of CO2 Sequestration Using Portland Cement in Geological Reservoir Based on Unified Pipe-network Method, Energies, 13, https://doi.org/https://doi.org/10.3390/en13020387, 2020.

Zehe, E., Loritz, R., Edery, Y., and Berkowitz, B.: Preferential Pathways for Fluid and Solutes in Heterogeneous Groundwater Systems: Self-Organization, Entropy, Work, Hydrol. Earth Syst. Sci., 25, 5337–5353, https://doi.org/https://doi.org/10.5194/hess-25-5337-2021, 2021.

Zhang, Y., Cao, Z., Hou, F., and Cheng, J.: Characterizing Preferential Flow Paths in Texturally Similar Soils under Different Land Uses by Combining Drainage and Dye-Staining Methods, Water, 13, https://doi.org/https://doi.org/10.3390/w13020219, 2021.

Zhang, Z. and Chen, Q.: Comparison of the Eulerian and Lagrangian methods for predicting particle transport in enclosed spaces, Atmospheric Environment, 41, 5236–5248, https://doi.org/https://doi.org/10.1016/j.atmosenv.2006.05.086, 2007.